Developing a compressor, fan, and active grille shutter control strategy for air conditioner duty cycles to improve overall vehicle power consumption

By

Trevor Parent

A Thesis
Submitted to the Faculty of Graduate Studies
through the Department of Mechanical, Automotive, and Materials Engineering
in Partial Fulfillment of the Requirements for
the Degree of Master of Applied Science
at the University of Windsor

Windsor, Ontario, Canada

2022

ABSTRACT

Fuel consumption optimization is a critical field of research within the automotive industry to meet consumer expectations and regulatory requirements. A reduction in fuel consumption can be achieved by reducing the energy consumed by the vehicle. Several subsystems contribute to the overall energy consumption of the vehicle, including the air conditioning (A/C) system. The loads within the A/C system are mainly contributed by the compressor, condenser fan, and underhood aerodynamic drag, which are the components targeted for overall vehicle energy use reduction in this research. It is essential to reduce the energy use of these components, as it will reduce the overall vehicle energy use and improve the vehicle's fuel economy. There is ongoing competition within the automotive industry for manufacturers to achieve the best possible fuel economy. This research explores a new avenue for A/C system control by considering the condenser fan power and the power consumption due to vehicle drag (regulated by the condenser fan and active grille shutters (AGS)) to reduce the energy consumption of the A/C system and improving the overall vehicle fuel economy. The control approach used in this paper is model predictive control (MPC), which uses a model of the vehicle A/C system to make predictions about the behaviour of the real system. The industrial partner provided a model of the A/C system that is further improved and validated for this work. The controller is designed in Simulink, where the compressor clutch signal, condenser fan speed, and AGS open fraction are considered as inputs. The controller is then connected to GT-Suite (which contains the actual vehicle plant model) to form a software-in-the-loop (SiL) simulation environment, where the controller sends actuator inputs to GT-Suite, and the vehicle response is sent back to the controller in Simulink.

TABLE OF CONTENTS

LIST OF FIGURES

LIST OF TABLES

CHAPTER 1
INTRODUCTION

This thesis is written in a manuscript style, meaning the major chapters within this paper each represent a published, or planned to be published work. In this research, a mathematical model for the A/C system of a conventional gasoline vehicle is extended from previous works. A model predictive controller (MPC) is developed and utilizes the extended A/C system model as the internal prediction model. The outcome of this work is to assess the benefit, if any, to including additional actuating inputs, namely the active grille shutters (AGS), to the A/C system control scheme. The power consumption and temperature tracking performance of the MPC will be compared with the previous baseline controls approach.

1.1 Objective and High-Level Approach

In short, the problem to be solved includes the following objectives:

Objective 1. Developing and validating an extended model of the A/C system in MATLAB/Simulink

Objective 2. Developing an MPC that regulates the temperature of the air sent to the vehicle's cabin by controlling the compressor clutch, fan angular speed, and AGS position in the A/C system to reduce the overall vehicle power consumption by considering the power consumed by the compressor, fan, and vehicle drag

1.2 Thesis Outline and Overview of Contributions

This thesis is divided into two major chapters:

- **Chapter 2: Nonlinear modelling of an air conditioning system with consideration to underhood aerodynamic drag and overall power consumption**

  This chapter describes a mathematical modelling method for an A/C system considering additional actuating inputs for the intention of control scheme implementation. A nonlinear model is provided by the industrial partner and is extended to consider a model of the aerodynamic vehicle drag caused by vehicle driving speed, AGS angle, and condenser fan rotational speed. The model is presented and validated against a high-fidelity virtual model of the vehicle. The resulting nonlinear model created will be used for the MPC controller development in Chapter 3.

- **Chapter 3: Developing a compressor, fan, and active grille shutter model predictive control strategy for air conditioner duty cycles to improve overall vehicle power consumption**

  In this chapter, an MPC algorithm is developed to control an A/C system by manipulating three actuating inputs: the compressor clutch, condenser fan rotational speed, and the AGS angle. The MPC scheme makes use of the nonlinear model derived in Chapter 2 as an internal plant model. The objective of the controller is to maintain satisfactory setpoint tracking for the air temperature entering the vehicle cabin while attempting to reduce the overall power consumed by the actuating components, as well as vehicle aerodynamic drag.

Finally, Chapter 4 contains concluding remarks and potential avenues for future work that can be conducted to further advance the contributions of this paper in the field of A/C system modelling and control design.

CHAPTER 2
NONLINEAR MODELLING OF AN AUTOMOTIVE AIR CONDITIONING SYSTEM WITH CONSIDERATION TO UNDERHOOD AERODYNAMIC DRAG AND OVERALL POWER CONSUMPTION

2.1 Introduction

Automotive air conditioning (A/C) systems are often modeled mathematically to demonstrate the performance and behavior of their components as the system attempts to cool the vehicle's cabin. State-of-the-art models for A/C systems consider the compressor and condenser fan as controllable actuators to maintain cabin comfort. In work published to date, the consideration of the active grill shutters (AGS) as a controllable actuator is not present [1]–[3]. The AGS impacts the cooling performance of the A/C system, as it provides an additional mechanism to control airflow through the condenser at a given vehicle speed in addition to the fan rotational speed [4], [5]. The amount of underhood flow also affects vehicle drag, which can be accounted for via the power consumption of the A/C system [6], [7]. Many mathematical models of A/C systems are developed with the intention of control implementation, with the reduction of energy consumption considered a primary objective [8]. Most models used by controllers in academic literature only consider the compressor and condenser fan as controllable actuators since those have a high power consumption [9], [10]. The model presented in this paper builds upon the state-of-the-art by introducing the AGS as a controllable actuator to regulate the front-end airflow and considers the underhood vehicle airflow drag effects on the power consumption of the vehicle. This paper thus presents a holistic model for the automotive A/C system power consumption.

The novelty of this work is in *extending an A/C system model completeness by considering front-end air flow cooling effects and power consumption comprising of:*

1. Improving the completeness of the vehicle A/C nonlinear model by adding the impact of the AGS on the determination of the underhood air flow
2. Developing a holistic model for the A/C system power consumption by considering underhood aerodynamic drag effects

3. Creating a fan power consumption model that captures the impact of changing rotational speed and volumetric air flow rate

The remaining sections of this paper are organized as follows. Section 2.2 outlines the details of the system being modeled, the underlying mathematical model used to develop the extended model formulated in this work, and the new advancements to previous modeling work done in the literature [11]. Section 2.3 includes the validation of the nonlinear (NL) model with the higher-fidelity vehicle energy management (VEM) model, an analysis of the holistic power consumption model, a demonstration of the nonlinear model's ability to react to imposed step inputs, and a discussion of the results.

In this paper, several models are referenced throughout. In order to maintain clarity and consistency, a short summary and comparison of the two models is introduced in Table 1.

Table 1: Model summary and comparison

Model Name	VEM	NL
Brief Model Description	High-fidelity vehicle dynamics model created using Gamma Technologies (GT) Suite [1] representing the real physical vehicle.	Nonlinear model implemented in Simulink based on equations (2) and (4).
Pros	Holistic model of entire vehicle, including all subsystems such as powertrain, A/C, cabin, electrical, etc.	Can accurately capture trends
Cons	High computational cost and slow runtime due to model complexity	Unable to run as a standalone model since it requires inputs in the form of time-series data from VEM model output

2.2 Materials and Methods

2.2.1 Description of A/C System Model

Figure 1 depicts a simplified block diagram of the A/C system, showcasing the connection of components, the flow of air and refrigerant, and the mathematical variables discussed in the underlying mathematical model of the system in section 2.2.4.

The four main components along the A/C system's refrigerant loop are the compressor, condenser, expansion valve, and evaporator. To develop a complete model of the A/C system, component models must capture the behavior of these four components. This paper

describes such a model for implementing a controller for reducing energy consumption in future work. The controller will regulate the system to send the correct air temperature to the cabin while minimizing the power consumption of the A/C system. The heat exchanger (HEX) pressures are the minimum quantities needed to fully describe the behavior of this system and are chosen as the state variables. The model thus is formed as:

$$\begin{aligned} \dot{p}_c &= f_1\left(p_c, \pi_c, N, X, \dot{m}_{ref}, T_{air,in,c}, h_{in}, v\right) \\ \dot{p}_e &= f_2\left(p_c, p_e, \pi_c, \dot{m}_{ref}, Q_e, T_{air,in,e}\right) \end{aligned} \tag{1}$$

where p_c and p_e are the refrigerant pressures in the condenser and evaporator, π_c is the compressor clutch engagement (on/off), N is the rotational speed of the condenser fan, X is the open-fraction of the AGS, $\dot{m}_{ref}$ is the refrigerant mass flow rate, Q_e is the volume flow rate of the air from the blower fan, $T_{air,in,c}$ and $T_{air,in,e}$ are the inlet air temperatures to the condenser and evaporator, h_{in} is the inlet enthalpy to the condenser, and v is the vehicle speed. Models for f_1 and f_2 based on the behavior of the refrigerant are described in section 2.2.4. Since the intended usage of the model is within a control scheme to reach the target cabin temperature with minimum energy consumption, we also develop models of the energy consumption of the overall A/C system, including additional drag due to underhood flow, in section 2.2.7. The inclusion of the impact of the AGS on underhood airflow and of the increase in power consumption associated with drag caused by that underhood flow are the key advancements over the state-of-the-art presented in this paper.

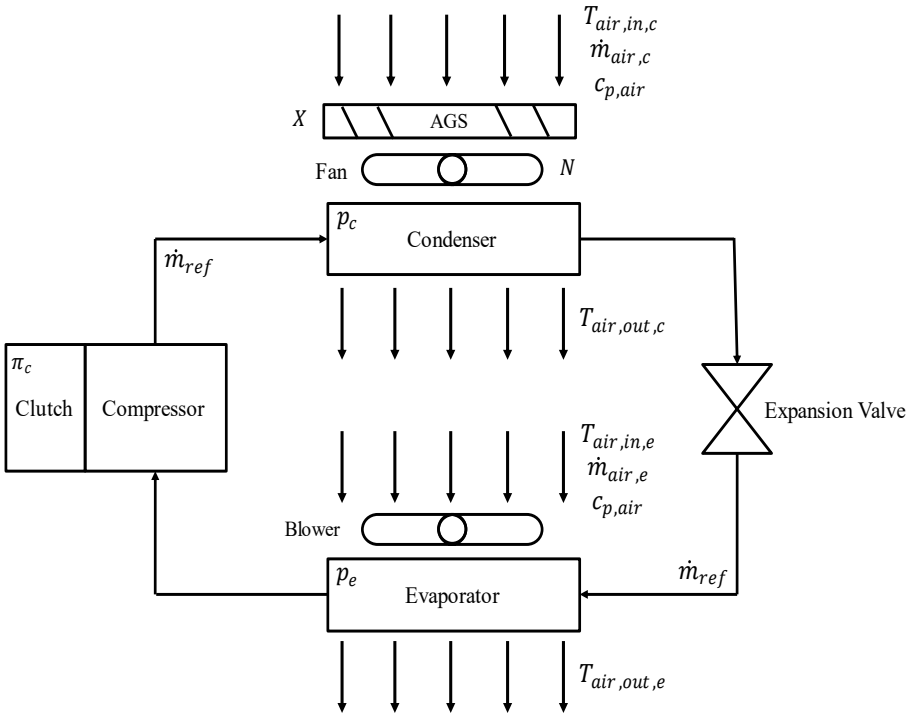

Figure 1: Simple A/C system diagram

2.2.2 Reference System

The controller will use the mathematical model to predict the behavior of a physical A/C system and send controlled inputs (compressor clutch, condenser fan rotational speed, and AGS open-fraction) to a high-fidelity VEM model developed by the industrial partner. This VEM model will act as a substitute for an actual physical vehicle for controller development; the output from the VEM model is treated as the output from the physical vehicle. Thus, the nonlinear models in this paper are validated against the VEM model.

2.2.3 Compressor

The VEM model provided by the industrial partner contains a virtual model of the compressor present in the physical vehicle. The VEM model uses the current baseline production controls to determine the compressor displacement, then provides a mass flow rate and outlet enthalpy value at each time step throughout the drive cycle. The control scheme intended to use our model controls the on/off command for the compressor clutch. Thus, modeling the compressor mass flow rate is unnecessary as it already exists in the VEM model and can be provided as input to the model. As an extension to the work

presented in this paper, the mass flow rate could be modeled from the first principles to eliminate the need for a VEM model connection. However, in the case of this paper, the VEM model is used since the intention of this model is for usage in control architecture development.

2.2.4 Heat Exchangers

The two HEXs in the A/C system are the condenser and evaporator, where the refrigerant undergoes phase changes between liquid and vapor states. The mathematical models of these two HEXs must capture this change in thermodynamic state. The underlying HEX mathematical equations were derived from first principles and provided by the industrial partner based on work described in [2]. The work in [2] [2]provides a simplified method to obtain a mathematical model for the HEX pressure by assuming a two-phase flow (liquid and gaseous) and approximating the thermodynamic states at the inlet and outlet of each HEX by relating it to the saturated liquid and vapor conditions. At the condenser outlet, the refrigerant is a saturated liquid. At the evaporator inlet, the refrigerant is assumed to have the same enthalpy as the refrigerant at the condenser outlet. The pressure at the inlet and outlet of the evaporator are equal, with a 10°C superheat at the evaporator outlet maintained by the expansion valve. This will be further discussed in section 2.2.5. The full derivation of the nonlinear pressure equations is available in [2], which results in the final forms:

$$\dot{p}_c = \frac{\left[Q_c \rho_a c_{p,air}(T_{air,in} - T_{air,out}) + \pi_c \dot{m}_{ref}(h_{in} - h_{out})\right]}{V\left[(1-\bar{\gamma})\frac{\partial(\rho_l h_l)}{\partial p} + \bar{\gamma}\frac{\partial(\rho_g h_g)}{\partial p} + (\rho_g h_g - \rho_l h_l)\frac{\partial \bar{\gamma}}{\partial p} - 1 + \frac{m_H c_H}{V}\left(\frac{\partial T_{wall}}{\partial p}\right)\right]}$$

$$\dot{p}_e = \frac{\left[Q_e \rho_a c_{p,air}(T_{air,in} - T_{air,out}) + \pi_c \dot{m}_{ref}(h_{in} - h_{out})\right]}{V\left[(1-\bar{\gamma})\frac{\partial(\rho_l h_l)}{\partial p} + \bar{\gamma}\frac{\partial(\rho_g h_g)}{\partial p} + (\rho_g h_g - \rho_l h_l)\frac{\partial \bar{\gamma}}{\partial p} - 1 + \frac{m_H c_H}{V}\left(\frac{\partial T_{wall}}{\partial p}\right)\right]} \quad (2)$$

where Q_c is the volume flow rate of the air through the condenser, ρ_a is the air density, h_{out} is the outlet refrigerant enthalpy, $T_{air,out}$ is the outlet air temperature, ρ_l, h_l, ρ_g, h_g are the densities and enthalpies for the refrigerant calculated at saturated liquid and vapor states, c_H is the specific heat of the HEX material, $c_{p,air}$ is the specific heat of air at constant pressure, $\overline{\gamma}$ is the mean void fraction of the refrigerant, V is the volume of the

HEX, m_H is the material mass of the HEX, and T_{wall} is the wall temperature of the HEX. The constant values for the HEX and fluid properties are detailed in Appendix A. The derivation of polynomial models for the refrigerant thermodynamic properties is detailed in section 2.2.6.

The second main aspect of this NL model is the temperature of the air leaving the evaporator, which is sent to the cabin for cooling. The air temperature depends on the temperature difference between the refrigerant temperature and air temperature passing through the evaporator, as well as the Nusselt number. A general model for the temperature of the air exiting a heat exchanger (condenser/evaporator) is given by:

$$\begin{aligned} T_{air,out,c} &= f_1\left(T_{ref}, T_{air,in}, NTU\right) \\ T_{air,out,e} &= f_2\left(T_{ref}, T_{air,in}, NTU\right) \end{aligned} \tag{3}$$

where T_{ref} is the HEX refrigerant temperature and NTU is the number of transfer units of the air. The final model of the air temperature in [2] is:

$$\begin{aligned} T_{air,out,c} &= T_{ref,c} + \left(T_{air,in,c} - T_{ref,c}\right)^{(-NTU_c)(K_{ca})} \\ T_{air,out,e} &= T_{ref,e} + \left(T_{air,in,e} - T_{ref,e}\right)^{(-NTU_e)(K_{ea})} \\ NTU &= \frac{\alpha A_s\left[1 - F_{fin}(1 - \eta_{FA})\right]}{\dot{m}_a c_{p,air}} \end{aligned} \tag{4}$$

where α is the convective heat transfer coefficient of the air, A_s is the external surface area of the HEX, F_{fin} is the fraction of air-to-structure surface area on the fins, η_{FA} is the air-side fin efficiency, $\dot{m}_a$ is the mass flow rate of the air, and K_{ca} and K_{ea} act as multipliers on the Nusselt number. As stated earlier, the derivation of polynomial models for the refrigerant thermodynamic properties, such as $T_{ref,c}$ and $T_{ref,e}$, are detailed in section 2.2.6.

The industrial partner provided computational fluid dynamics (CFD) data related to the specific vehicle of interest for this project, which included air flow rate values measured at various combinations of vehicle speed, fan rotational speed, and AGS open-fraction. A multiple linear regression method was used to create a model for the condenser air flow rate function based on this data.

A second-order regression model is the simplest model order that makes sense physically. A linear model would have three terms: one for the AGS open-fraction, fan

rotational speed, and vehicle speed. When the fan speed and vehicle speed are zero, the linear AGS term will cause a nonzero flow rate to be predicted by the model, which does not make sense physically, so the model does not include a linear AGS term. Thus, a second-order model with cross terms is the simplest model able to include the effect of all three inputs affecting the airflow. The second-order model provided a good fit to the data, with an R^2 value of 0.9981. Model orders higher than two were created and tested, but none provided a significant improvement to the goodness of fit to the data; thus, a model order of two was used.

The model takes the form:

$$Q_c = 0.07722\widehat{N} + 0.01057v + 4.913 \times 10^{-5}v^2 + 0.2039X\widehat{N} + 0.002671Xv \quad (5)$$

where Q_c is the volume flow rate of the air in m^3/s, $\widehat{N}$ is the normalized rotational speed of the condenser fan between zero and one, X is the open-fraction of the AGS between zero and one, and the vehicle speed, v, is in m/s.

2.2.5 Expansion Valve

As mentioned previously, the thermodynamic states at the inlet and outlet of the HEXs are approximated based on the saturated liquid and vapor states. A similar assumption was introduced in [2] for modeling the expansion valve. The expansion valve regulates the refrigerant superheat temperature at the exit of the evaporator using a sensing bulb to maintain a constant superheat of 10°C to the refrigerant at the evaporator exit. This means the refrigerant conditions at the evaporator exit can be related to the saturated conditions of the refrigerant pressure level inside the evaporator. The modeling approach used in [2] also assumes that the enthalpy at the inlet of the evaporator is equal to the enthalpy at the outlet of the condenser, meaning there is no heat loss across the expansion valve.

2.2.6 Refrigerant Temperature

In this paper, to model the thermodynamic properties of the refrigerant, a linear least-squares regression method was used to fit continuous curves to discrete refrigerant property data from [3]. The range of pressure data used for the curve fitting is equal to the standard operating range of each HEX, as defined by the industrial partner. An example of one of the resulting polynomial models is:

$$T_{ref,c} = 8.4 \cdot 10^{-9} p_c^3 - 4.9 \cdot 10^{-5} p_c^2 + 0.12 p_c - 34.9 \quad (6)$$

where $T_{ref,c}$ is the temperature of the refrigerant leaving the condenser and p_c is the condenser refrigerant pressure. The full list of fitted curves are presented in Appendix A in equations (44)-(47). As mentioned earlier, this modeling work is intended for controller development. In this case, these polynomial curves must retain their accuracy when linearized for use in linear control approaches. When conducting curve fitting to a data set, the possibility of large oscillations occurring at either side of a discrete data point increases as the order of the polynomial increases. This is called Runge's phenomenon [4]. To ensure that this problem does not arise for this model, the first derivative was compared with the numerical first differences between data points. Using polynomial functions instead of lookup tables results in less effort during the linearization of the model to compute the derivatives. This is owed to the fact that the derivatives of lookup tables may be unavailable for discrete datasets. After replacing the lookup tables with the polynomial equations, the root mean squared error (RMSE) for the system output had only a 0.1°C increase. The RMSE definition used for this purpose is formed as:

$$RMSE = \sqrt{\frac{\sum_{i=1}^{n_{points}} \left(x_{actual,i} - x_{model,i}\right)^2}{n_{points}}} \quad (7)$$

where $x_{actual,i}$ is the variable value from the data, $x_{model,i}$ is the variable value from the model, and n_{points} is the total number of data points. To assess the impact of this change, the RMSE was normalized by the range of the data set, resulting in a normalized RMSE of 0.19%.

2.2.7 Power Consumption

The control design that will use this model will be utilized to reduce the power consumption of the A/C system. Thus, a model of the power-consuming aspects must be defined as well, that being the compressor, condenser fan, and power consumption due to aerodynamic drag associated with the underhood airflow. The compressor's power consumption is modeled from first principles using well-established thermodynamic and mechanical relationships from [5]. For brevity, the final form of the equation is given as:

$$\dot{W}_{comp} = \frac{\dot{m}_{ref}(h_{out} - h_{in})}{\eta_{comp}} \tag{8}$$

where $\dot{m}_{ref}$ is the mass flow rate of the refrigerant, h_{in} and h_{out} are the enthalpies of the refrigerant at the inlet and outlet of the compressor, and η_{comp} is the ratio of isentropic efficiency to volumetric efficiency of the compressor.

The power consumption of the condenser fan is computed based on the underhood air flow and work done by the fan. From the Euler turbine equation, this is:

$$\dot{W}_{fan} = \rho_a Q_c \Delta h_t \tag{9}$$

where $\dot{W}_{fan}$ is the power consumption of the fan and Δh_t is the stagnation enthalpy change across the fan. The enthalpy change across the fan is not explicitly known, but data has been provided by the industrial partner for the fan pressure rise and adiabatic efficiency. For low-speed incompressible flow of a perfect gas, the stagnation enthalpy change can be expressed in terms of the fan pressure rise and efficiency:

$$\Delta h_t = \frac{\Delta p_t}{\rho_a \eta_{fan}} \tag{10}$$

where Δp_t is the pressure rise required of the fan and η_{fan} is the fan adiabatic efficiency. Substituting this expression into equation (9) yields the final form of the fan power equation:

$$\dot{W}_{fan} = \frac{\rho_a Q_c \Delta p_t}{\rho_a \eta_{fan}} = \frac{Q_c \Delta p_t}{\eta_{fan}} \tag{11}$$

Recall that a model for Q_c has been established and is given by equation (5). Thus, analytical expressions are needed for the fan pressure rise and efficiency to complete this fan power model. The industrial partner supplied experimental data for the fan pressure rise and efficiency at various underhood air flow rates for a fan speed of 2500 rpm. A relationship between the underhood air flow rate, fan pressure rise, and efficiency can be determined from this data, but it is only valid when the fan speed is at 2500 rpm. For this model, the flow is assumed to be incompressible. We neglect the effect of Reynolds number variations on efficiency and pressure rise. To enable scaling of the power consumption model for any fan rotational speed, the pressure rise and air flow data were nondimensionalized to convert the experimental data from dimensional pressure rises and

flow rates to nondimensional pressure rise coefficients and flow coefficients. The form of these nondimensional parameters are expressed as:

$$\phi = \frac{U_x}{U_m} = \frac{\left(\frac{Q_c}{A_{fan}}\right)}{N r_m \left(\frac{2\pi}{60}\right)} \qquad (12)$$

$$\psi = \frac{\Delta p_t}{\rho_a U_m^2}$$

where ϕ is the flow coefficient, ψ is the pressure rise coefficient, U_x and U_m are the axial and midspan blade speeds, A_{fan} is the cross-sectional flow area of the fan, N is the rotational speed of the fan in rotations per minute, and r_m is the midspan radius of the fan. Two polynomial equations were developed by using a least-squares regression method to fit polynomial equations to the nondimensionalized experimental data, shown in Figure 2. In Figure 2, the fan efficiency has been normalized by the highest fan efficiency provided in the experimental data.

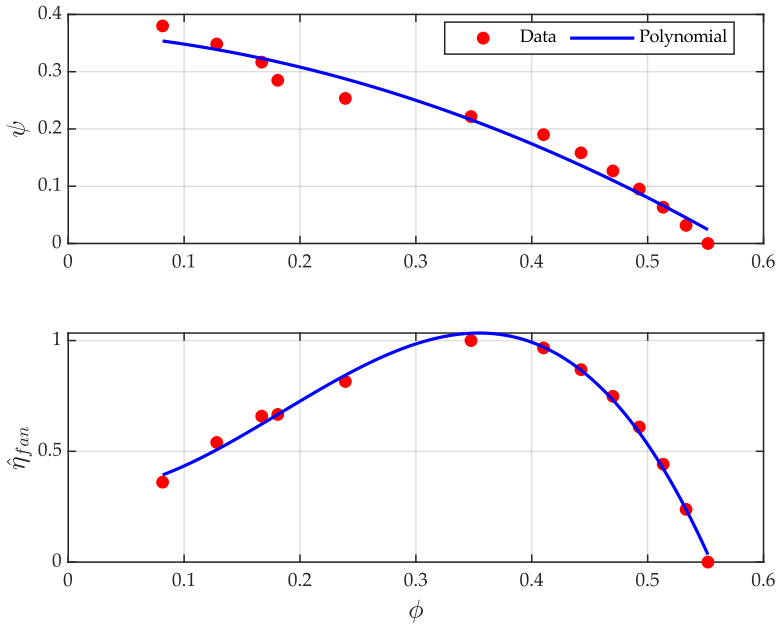

Figure 2: Pressure rise coefficient and normalized fan efficiency data with polynomial fits

These two polynomials relate the pressure rise coefficient and the efficiency of the fan to the flow coefficient of the underhood airflow and are given by:

$$\psi = -0.897\phi^2 - 0.132\phi + 0.3703 \qquad (13)$$

$$\eta_{fan} = -14.82\phi^3 + 8.20\phi^2 - 0.226\phi + 0.133$$

The pressure rise coefficient and efficiency are found using the expressions above after non-dimensionalizing the flow rate. Thereafter, the pressure rise is calculated by dimensionalizing the pressure rise coefficient and used with the efficiency and dimensional flow rate in equation (11) to calculate the fan power.

As an extension to the previous modeling work from [2] and [5], a model was created to evaluate the power consumption associated with additional drag on the vehicle due to underhood airflow, which is set by the vehicle speed, fan rotational speed, and AGS open-fraction. The model for this power consumption is:

$$\Delta\dot{W}_{drag} = \frac{1}{2}\rho_a A_{fr} v^3 \Delta C_d \tag{14}$$

where, A_{fr} is the frontal area of the vehicle, and ΔC_d is the increase in drag coefficient due to additional flow through the underhood at a given vehicle speed due to the AGS being open and/or the fan being on.

To create a model for the drag coefficient, the industrial partner supplied experimental data for drag coefficient as a function of underhood air volume flow rate at a constant vehicle speed of 67 mph. Since the data for the drag coefficient was only available for a single vehicle speed, the model for the underhood air volume flow rate in equation (5) was normalized by the vehicle speed. The weak impact of vehicle speed on the flow rate can be observed by dividing equation (5) by v. A linear least squares regression method was used to create a polynomial fit for the drag coefficient as a function of normalized flow rate from the experimental data:

$$C_d = 0.042872\left(\frac{Q_a}{v}\right) + 0.3554 \tag{15}$$

where the RMSE is 0.000419. As mentioned earlier, the increase in drag coefficient relative to the flow rate achieved when the AGS is closed and the fan is off is computed and used in equation (14) to calculate the additional power required due to the increase in drag on the underhood of the vehicle.

2.2.8 Model Implementation

To implement the NL model in MATLAB/Simulink, drive cycle parameters and initial conditions were coded in MATLAB to create a set of input parameters used to simulate the

model. The drive cycle parameters include the vehicle speed profile, ambient air conditions, etc. The mathematical equations (2) and (4) are implemented in Simulink to create a model of the A/C system. A subsystem model for each HEX was created with its specific equation outlined in equations (2) and (4), along with the HEX physical properties to fully recreate the mathematical expressions shown in equations (2) and (4). The thermodynamic state of the refrigerant at the outlet of the condenser model is sent directly to the evaporator model to be used as inputs. The VEM model is connected in place of a compressor model, and the former sends the compressor outputs to Simulink. The MATLAB script initializes the drive cycle conditions, then executes the NL model in Simulink and records the results.[2]

2.2.9 Heat Exchanger Multiplier Parameter Calibration

As mentioned, there can be significant uncertainty in modeling the convective heat transfer and Nusselt number. The Nusselt number was tuned for each HEX by adding a coefficient, denoted as K_{ca} and K_{ea} for the condenser and evaporator, respectively. A grid search method was used to find the combination of coefficient values that reduced the RMSE for the NL model output, which is the air temperature leaving the evaporator, $T_{e,air,out}$. This optimization yielded a minimum normalized RMSE value of 3.4%, with a K_{ca} value of 0.29 and a K_{ea} value of 0.55. The normalized RMSE was calculated by dividing the RMSE found using equation (7) by the air temperature range. This is an improvement from the normalized RMSE of the original model in [2] (with no multipliers) of 5.4%.

2.3 Results

The mathematical models outlined in section 2.2 were all implemented in Simulink to assess the performance of the A/C system. The calibration data came from VEM model data for the SC03 drive cycle, a standard drive cycle used by the Environmental Protection Agency (EPA) to assess vehicle fuel economy [7]. To be clear, the NL model implemented in Simulink is not able to be simulated as a standalone model. In order to simulate the NL model, timeseries profiles for the controlled inputs ($\pi_c, \widehat{N}, X$) and external (uncontrolled) inputs ($\dot{m}_{ref}, Q_e, T_{air,in,c}, T_{air,in,e}, h_{in,c}, v, h_{out,e}$) must be provided to the NL model, since the NL model does not compute these on its own. The model has been implemented in this way due to its intended usage for control development, where it will accept external signals

from the VEM model. The comparison between the nonlinear and VEM models for the SC03 cycle is shown in Figure 3. The comparison shown in Figure 3 demonstrates that the NL model is a good approximation of the behavior of the high-fidelity VEM model designed by the industrial partner, which is treated as the benchmark system in this case. For neatness, the vehicle speed input has been presented in a normalized form:

$$\hat{v} = \frac{v}{v_{max}} \tag{16}$$

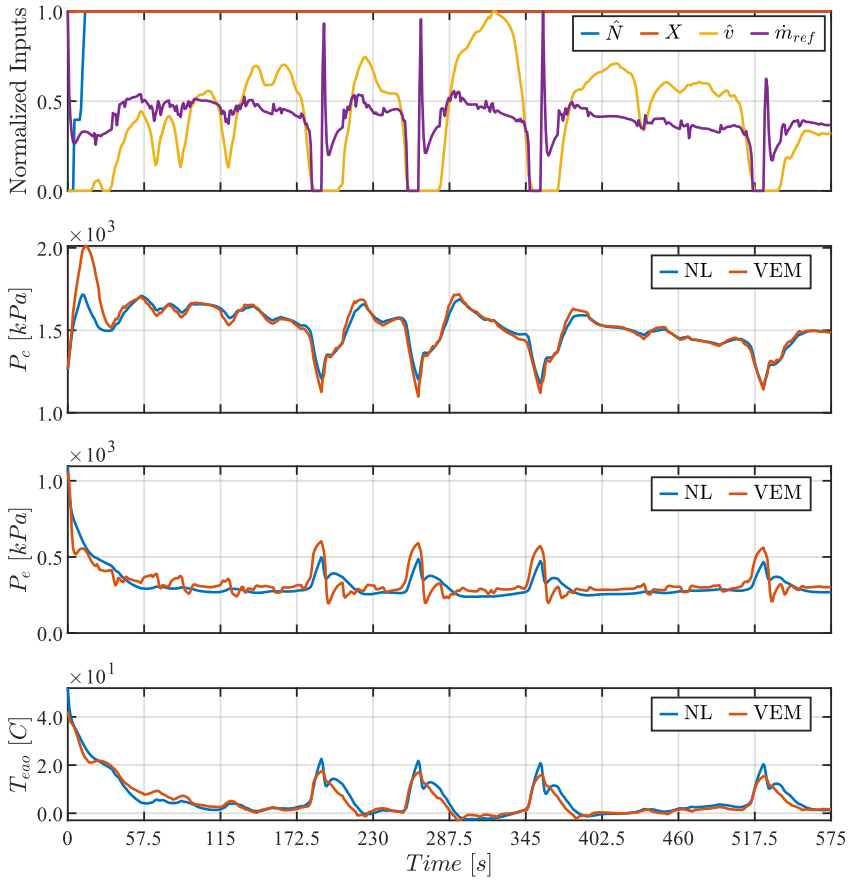

Figure 3: VEM and NL pressure and temperature comparison for SC03 cycle

The normalized RMSE between the VEM and NL model signals shown in Figure 3 are displayed in Table 2. The error between the two models can be explained by approximations made in the NL model, such as curve fitting for the refrigerant thermal properties and underhood airflow. It can be seen that the evaporator pressure of the NL model has more inertia when comparing the transient portions of the response. The stiffness of the evaporator pressure of the NL model can be attributed to the multiplier, K_{ea},

introduced for the Nusselt number for the convective heat transfer. As the tuning parameter is increased, the average agreement with the NL and VEM models improves, but the transient behavior slows. For example, when the multiplier value is increased, the NL curve is shifted upward and compressed. Future research into this modeling can improve the response by investigating other methods to account for uncertainties with convective heat transfer modeling. To further assess the NL model, it was also run for a custom drive cycle to observe the agreement with the VEM model performance. For this custom drive cycle, the condenser fan and AGS actuator inputs were varied to induce transients in the model response. For the first half of the cycle, the AGS was held fully open while the fan speed ramped from max speed to zero, then back to max speed. For the second half of the cycle, the fan speed and AGS open-fraction were varied quasi-randomly to induce more transients in the model performance. The comparison between the NL model and the VEM model for this custom drive cycle is shown in Figure 4.

The normalized RMSE between the VEM and NL model signals shown in Figure 4 are displayed below in Table 2, demonstrating the NL model's ability to handle transients arising from the inputs. It can be observed from Figure 3 and Figure 4 that the spikes in the refrigerant mass flowrate yield the greatest local error between the NL and VEM behaviors, causing the normalized RMSE to increase.

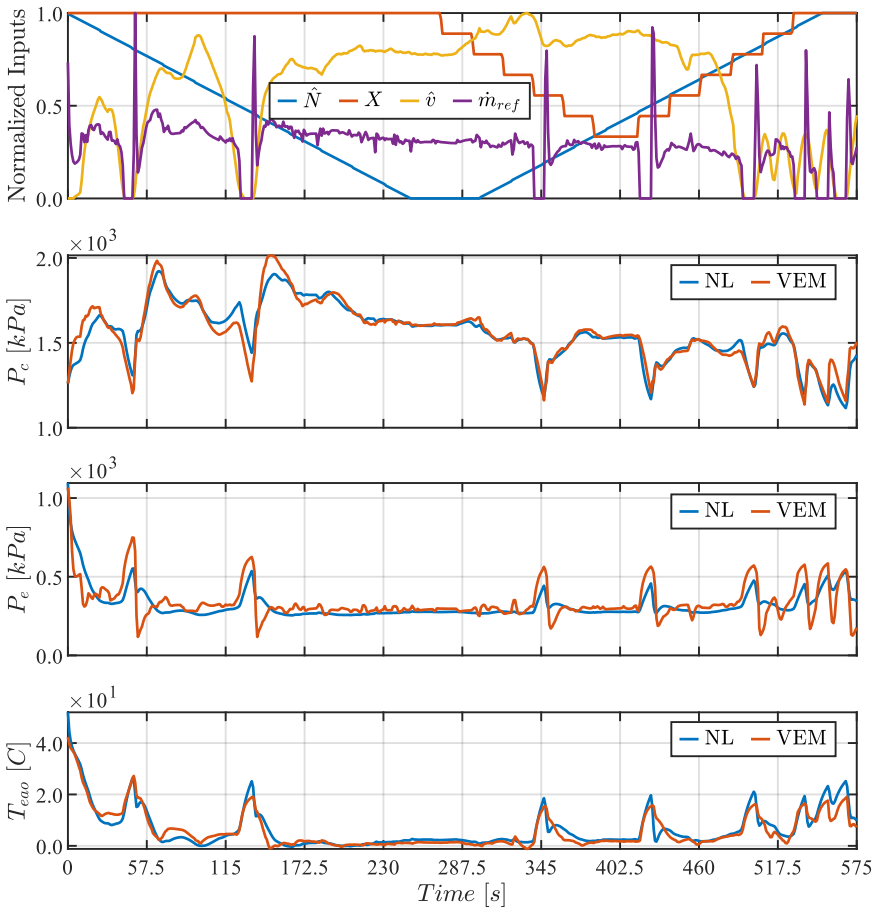

Figure 4: VEM and NL pressure and temperature comparison for custom drive cycle

Table 2: Normalized RMSE between VEM and NL models for SC03 and custom cycles

Parameter	p_c **[kPa]**	p_e **[kPa]**	T_{eao} **[C]**
SC03 Cycle Normalized RMSE	4.4%	7.2%	3.8%
Custom Cycle Normalized RMSE	6.5%	7.8%	4.6%

To further assess the accuracy of the model, the VEM and NL models were simulated using a constant vehicle speed profile of 13.4 m/s subject to an imposed fan speed step input from 2500 rpm to 0 rpm. For the entire cycle, the AGS is fully open, and the clutch is engaged. The results are shown in Figure 5. The same scenario was simulated using the opposite input step, where the fan speed is imposed from 0 rpm to 2500 rpm, shown in Figure 6. The ability of the NL model to correctly capture the settling time of the VEM model when subject to a step input from one of the controlled actuators, as well as the dynamics

influenced by the refrigerant mass flow rate is demonstrated. The RMSE for Figure 5 and Figure 6 are shown in Table 3.

Table 3: RMSE between VEM and NL models for fan step input simulations

Parameter	p_c **[kPa]**	p_e **[kPa]**	T_{eao} **[C]**
RMSE for Negative Fan Step Input	21.8	20.2	0.876
RMSE for Positive Fan Step Input	44.4	10.8	0.487

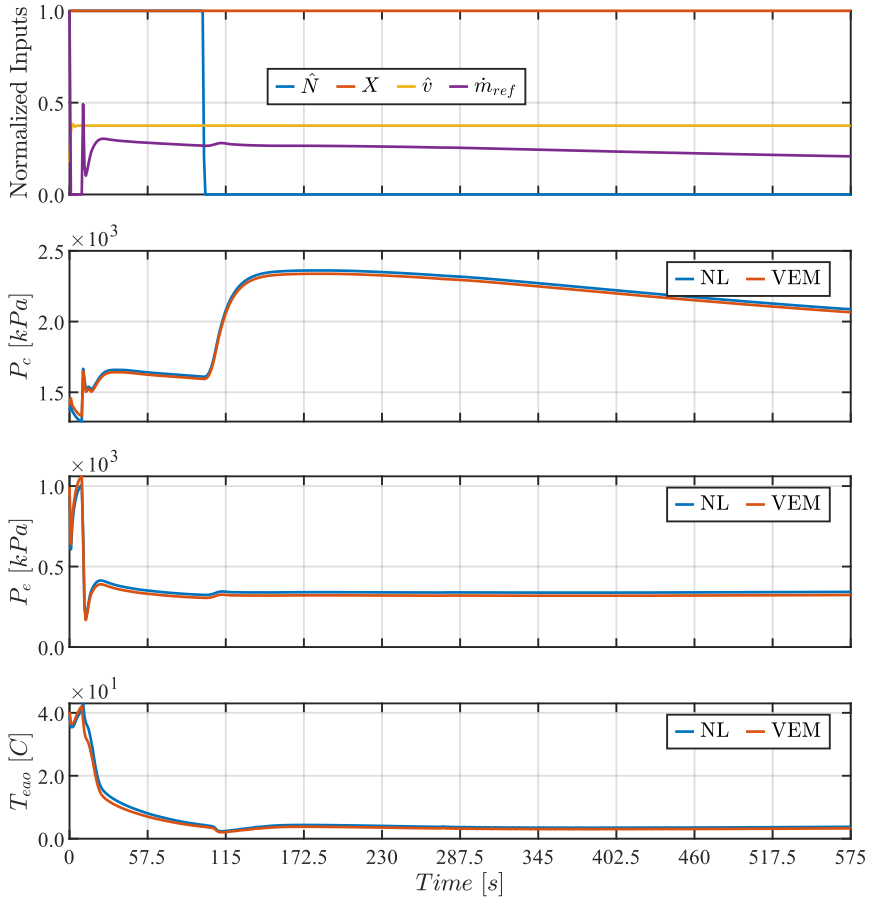

Figure 5: VEM and NL model comparison for fan speed step input – 2500 rpm to 0 rpm

The power consumption of the A/C system was assessed for the same driving conditions used to obtain the results displayed in Figure 3. To show how the power consumption assessment of the A/C system has been developed through this work, three comparisons are made: the power consumption of the VEM model, which only measures the compressor and fan power; the power consumption of the NL model using the same fan power model

present in the VEM model, the power consumption of the NL model using equation (11) for the fan power, and the power consumption of the NL model using equations (11) and (14), including the additional drag power. This comparison is shown in Figure 7.

From Figure 7, it can be seen that the VEM and NL - Baseline models have a good agreement for the total power consumed, which comes from the compressor and fan in these cases. When the new fan power model from equation (11) is used instead of the VEM fan power model, there is a slight increase in the total power. One of the main takeaways from this figure is that the power consumption associated with additional aerodynamic underhood drag is very small. This means that when additional cooling is required, opening the AGS will provide extra cooling at a small cost compared to other actuators, such as the fan and compressor.

The energy consumptions computed in each model are compared in Table 4. When the new fan power model in equation (11) is added to the NL model, the total energy consumption is increased from 1284.2 kJ to 1336.6 kJ. This demonstrates that the baseline fan power model was underpredicting the fan power consumption. The additional power consumed due to aerodynamic drag provides only a small increase in the total energy consumption computed, increasing it from 1336.6 kJ to 1353.2 kJ. Since the additional energy consumed due to the opening of the AGS is small, the addition of the AGS as a controllable actuator provides a useful tradeoff to save energy elsewhere in the A/C system. When the AGS open fraction increases, the amount of flow entering the condenser increases, providing additional cooling to the system. When this happens, the compressor cooling effort can be reduced, saving energy usage of the compressor.

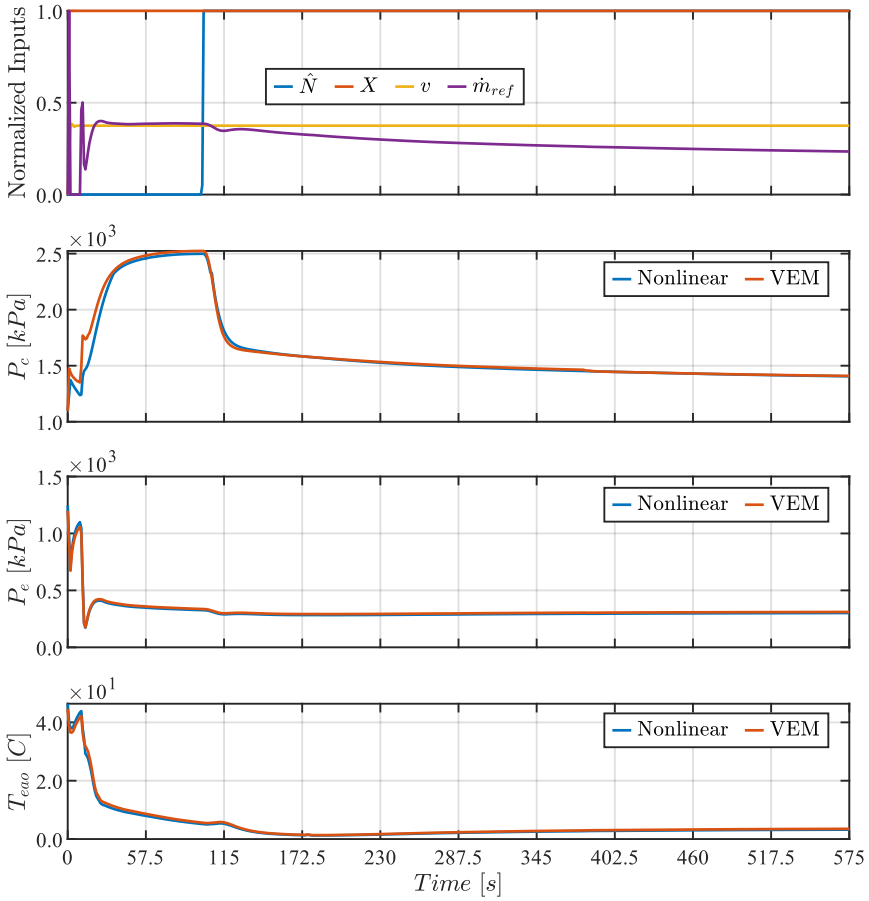

Figure 6: VEM and NL model comparison for fan speed step input – 0 rpm to 2500 rpm

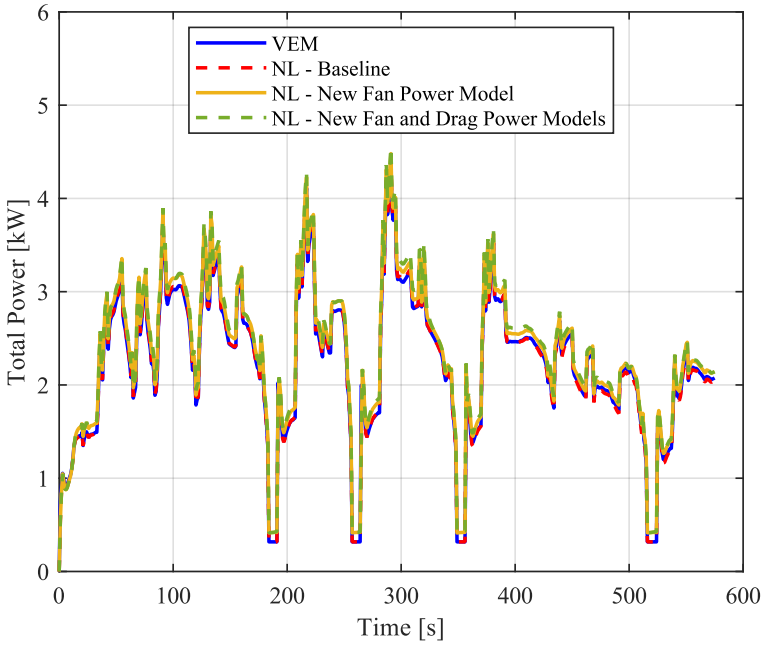

Figure 7: Total power consumption comparison for the SC03 drive cycle

Table 4: Energy consumption comparison for SC03 cycle

Model Name	VEM	NL – Baseline	NL – New Fan Power Model	NL – New Fan and Drag Power Models
Compressor Energy [kJ]	$1.11 \cdot 10^3$ (86.1%)	$1.10 \cdot 10^3$ (86.1%)	$1.10 \cdot 10^3$ (82.7%)	$1.10 \cdot 10^3$ (81.7%)
Fan Energy [kJ]	179 (13.9%)	179 (13.9%)	231 (17.3%)	231 (17.1%)
Drag Energy [kJ]	N/A	N/A	N/A	16.7 (1.2%)
Total Energy [kJ]	$1.29 \cdot 10^3$	$1.28 \cdot 10^3$	$1.34 \cdot 10^3$	$1.35 \cdot 10^3$
Percentage Change [%]	N/A	-0.200	3.87	5.16

To gain insight into the individual contributions each component has on the total power consumption in the NL model, the compressor, condenser fan, and additional drag power are presented individually in Figure 8.

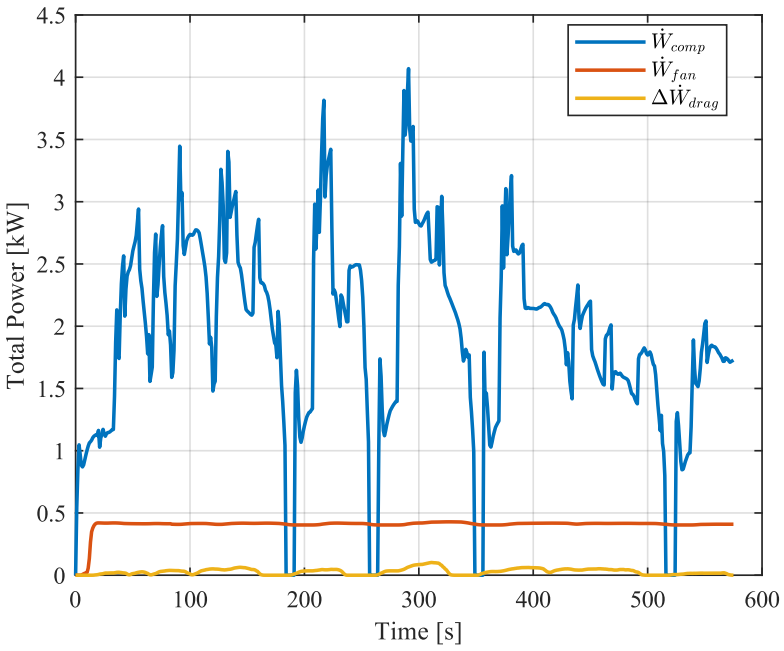

Figure 8: Compressor, condenser fan, and drag power consumption of NL model for SC03 cycle

The compressor power consumption is driven by the mass flowrate of the refrigerant, which has a very strong impact on the compressor power, as can be seen. The impact of

the volumetric airflow rate on the fan and additional drag power can also be seen. For the SC03 cycle shown in Figure 8, the fan speed and AGS positions are at their maximum physical values, that being 2500 rpm and fully open. Thus, any changes in the front-end airflow is caused by the vehicle speed, meaning the variations in the fan power and additional drag power observed in the figure are due to the change in vehicle speed.

Figure 9 depicts the combinations of AGS position and fan speed inputs to maintain a constant underhood flow rate of 450 cfm and the power consumption associated with the fan and drag. At this driving condition, the power consumed by the fan is clearly much greater than the power consumed due to additional underhood drag. The same analysis was conducted for conditions where the drag power was more significant, specifically when the vehicle speed is much higher. For these scenarios, the same findings were observed, where the fan power dominates the additional drag power. Figure 9 demonstrates that the same underhood air flowrate can be achieved using various combinations of AGS and fan inputs, but the power consumed is not constant. By opening the AGS, allowing more air to flow through the front-end of the vehicle, the fan can reduce its rotational speed to achieve the same cooling flow, but at a reduced power consumption. This will be useful for control implementation where cooling performance and power consumption reduction is of interest.

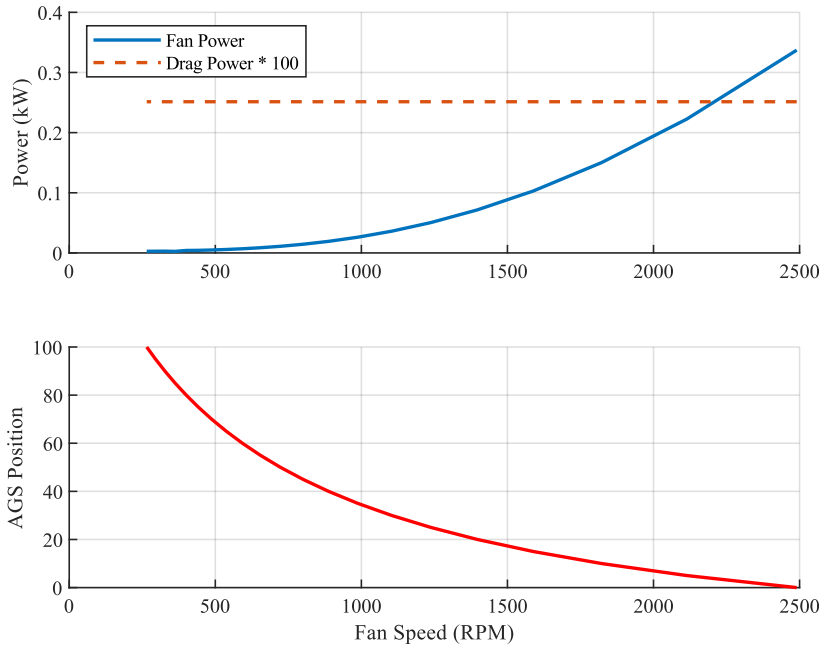

Figure 9: AGS position, fan speed, and power for 450 cfm air flow at 13.4 m/s vehicle speed

2.4 Conclusion

In this paper, we have considered the AGS as a controllable actuator to regulate the underhood airflow and power consumption due to the underhood drag. The modeling work described in [2] was extended by developing a model for the airflow through the vehicle's front end to allow the AGS actuation to be considered in the model. Models were created for the refrigerant thermodynamic properties, as well as the power consumption of the compressor, condenser fan, and underhood aerodynamic drag. The NL model was tuned to improve the agreement with various driving conditions, including the SC03 drive cycle and a custom drive cycle with strong transients in the controlled inputs. The NL model was validated against the behavior of a high-fidelity VEM model. The results showed that the overall performance of the system improved by reducing the error for the condenser pressure, evaporator pressure, and evaporator air temperature by 32.8%, 2.1%, and 2.6% respectively. It was found that the power consumption associated with additional drag on the vehicle due to underhood airflow is a very small contribution to the overall power consumed by the A/C system, only 1.2% for the SC03 cycle. This means that considering the AGS as a controllable actuator can be useful in terms of reducing the overall power consumption. By opening the AGS, additional cooling occurs due to the allowance of increased air flow through the vehicle's front-end, but only at a small power consumption cost. The cooling provided by the AGS air flow can reduce the cooling load on other actuators such as the fan. The outcomes of this work will be used in a controller design in future work where the compressor clutch, fan rotational speed, and AGS open-fraction will be controlled to reduce the overall energy consumption of the A/C system.

CHAPTER 3
DEVELOPING A COMPRESSOR, FAN, AND ACTIVE GRILLE SHUTTER MODEL PREDICTIVE CONTROL STRATEGY FOR AIR CONDITIONER DUTY CYCLES TO IMPROVE OVERALL VEHICLE POWER CONSUMPTION

3.1 Introduction

Every vehicle on the road is equipped with an A/C system that is used to regulate the temperature of the air travelling from the underhood of the vehicle to the vehicle cabin in order to maintain passenger comfort. It is a critical task to design a controller for the A/C system because without a controller, the operation of the A/C system, namely the circulating refrigerant, would solely depend on the operation of the engine of the vehicle, since the compressor is coupled to the engine. This means that the operation of the A/C system (and thus the control of the temperature of the air sent to the cabin) would be independent from what the passengers within the cabin request. The only way to increase the cooling effect would be to increase the speed of the vehicle, which is unsafe.

One of the earliest controller types employed for A/C system control was on/off controllers. This control technique was most commonly applied to the compressor clutch to engage and disengage the cooling loop to maintain the cabin temperature within a specific range [8]. These controllers are very simple to design and implement but do not account for energy-saving and can cause compressor wear due to frequent on/off cycling [9]. Feedback controllers were also used for A/C system control. Feedback controllers, such as proportional integral controllers, have demonstrated improvements in reducing the mechanical wear of the compressor by continuously controlling the variable displacement of the compressor [10]. Studies have shown difficulty with gain tuning for feedback controllers due to system nonlinearity and lack of consideration for energy use reduction since they only considered the evaporator coefficient of performance (COP) maximization [11]. A sliding-mode controller (SMC) developed by [12] reduced the chattering phenomenon of the compressor by controlling the compressor speed but did not consider the power consumption of the A/C system since the only output considered was the evaporator superheat temperature. Other SMCs have been shown to control the A/C system dynamics using linearized plant models but did not consider the power consumption of any components [13]. More recent developments in SMC applications to automotive A/C systems show potential

for energy savings of the compressor and fans, but these control methods still lack any consideration of vehicle drag and AGS control [14].

In recent years, MPC applications for A/C systems have seen more research interest in the academic sector. MPC is an exciting prospect for A/C system control. MPC makes predictions about the future behaviour of the system and corrects for deviations between the predicted and actual response since the optimal control sequence is updated at each time step [15]. MPC also lends itself well to A/C system control due to its ability to consider constraints on inputs, states, and outputs directly into the control problem formulation and is enforced by the controller [16]. Some of the earliest MPC formulations to A/C systems were seen for industrial refrigeration systems, primarily for supermarkets [17], [18]. These applications demonstrated that MPC techniques could be effectively used for A/C system control, but the main goal of these applications was to control the temperature of the goods within the storage facility, not energy consumption management [19].

More recently, MPC applications have been applied to automotive A/C systems. Most of the current literature on automotive A/C system control is investigated for hybrid electric vehicles (HEVs) and battery electric vehicles (BEVs) [20]. [21] proposed an MPC algorithm that minimizes the tracking error of the discharge air cooling power (cabin cooling requirement) and minimizes the energy consumption of the A/C system. However, this study considers the compressor power consumption to be the overall system energy consumption and did not consider radiator fan power or AGS control effects. [22] proposed a linearized MPC problem for a BEV to track the cabin temperature accurately. This nonlinear problem was reformulated into a linear quadratic cost function with linear constraints; this can lead to linearization error, but the question becomes, are we able to tolerate this error if it allows the problem to become much simpler and less computationally expensive (real-time application may be more feasible). [23] proposed a nonlinear MPC control for BEV/HEV to minimize power consumption. This approach demonstrated a 9% energy savings and accounted for power consumed by the blower (for the evaporator) but did not consider the AGS at all in the analysis. None of the MPC approaches have been applied to conventional vehicles in the literature reviewed for this research. Due to the several similarities existing between the A/C systems for electric and conventional vehicles, some of

the approaches and methodology used in these papers can be translated into gasoline vehicle applications. In most HEV and BEV studies, one of the primary design goals is the thermal management of the battery, which is something that is not needed for a conventional vehicle. Thus, since the intention of this work is for a conventional vehicle, the main focus can be on the thermal management of the cabin and overall vehicle power savings, without having to consider any sort of battery thermal management.

Several linear approximation MPCs have been formulated in the past, with the most popular being adaptive and gain-scheduled model predictive controllers [24] and [25]. These controller types will be discussed in more detail in section 3.2, but adaptive MPC is more promising for this application due to its effectiveness for control designs where the structure of the optimization problem (number of states and constraints) remains the same across different operating points.

The consideration of AGS control to reduce the overall vehicle power consumption and regulate the underhood airflow for cabin cooling has not been considered in any of the literature reviewed for this research. The AGS has a significant impact on the vehicle's thermal management. By opening the AGS, the refrigerant temperatures will decrease due to the additional airflow allowed into the underhood of the vehicle, which also decreases the cabin temperatures. This allows other components, such as the compressor, to reduce its working load and still satisfy the cooling requirements of the vehicle [26]. Although studies have shown that opening the AGS benefits underhood cooling, it comes at a cost. [27] demonstrated that as the AGS is opened, the drag force of the underhood vehicle airflow increases due to an increase in drag coefficient, concluding that the AGS has a significant impact on the fuel economy and power consumption of the vehicle. By controlling the condenser fan and AGS along with the compressor, it is expected that the energy used by the system can be further reduced. For example, by controlling the AGS angle, flow through the vehicle's front-end can be regulated and allow the fan to turn off completely to save power since the required airflow is supplied through the AGS. However, the drag changes associated with opening the AGS must also be factored in, as reducing A/C system energy use at the expense of higher fuel consumption to overcome drag would not be a desirable outcome. Thus, this paper extends previous work on model predictive control of automotive A/C systems by introducing the AGS as a new actuator into the control problem

and will also investigate the benefit to overall vehicle power consumption. The specification of the control problem extended by this work can be seen in Figure 10, where the blocks highlighted in red are the control interests in this paper.

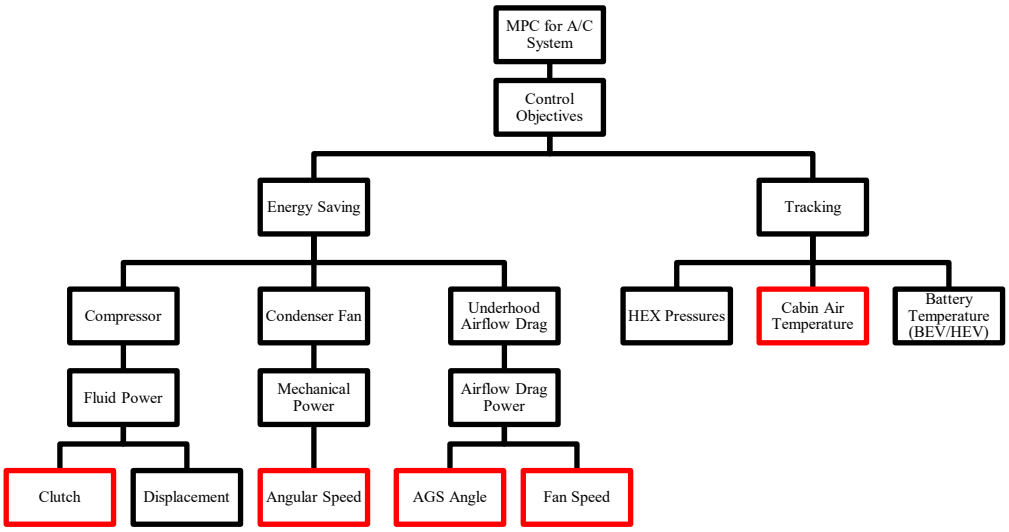

Figure 10: Visual tree of control problem of an A/C system

The novelty of this chapter is in *developing a model predictive control algorithm for gasoline vehicles that considers the control of the AGS to regulate the underhood airflow and reduce the overall vehicle power consumption.*

The remaining sections of this paper are organized as follows. Section 3.2 details high-level information related to MPC control formulations and discrete state-space system model forms. Section 3.3 includes a description of the linear problem formulation and control aspects such as the system states, inputs, outputs, physical limitations, and discretization. Section 3.4 outlines the quadratic programming formulation, which is the optimization technique used to solve the problem set up by section 3.3. Section 3.5 discusses the findings and implications of the MPC simulation results, as well as a discussion of the analysis. Section 3.6 concludes the chapter with some reflection, shortcomings, and avenues for future research.

3.2 MPC Description and Discrete State-Space General Form

MPC is a feedback control formulation that uses a mathematical model of a real system to make predictions about the system's future behaviour when influenced by a set of controlled actuating inputs. A simple block diagram of an MPC is shown in Figure 11 and the configuration of an MPC with a real system is shown in Figure 12.

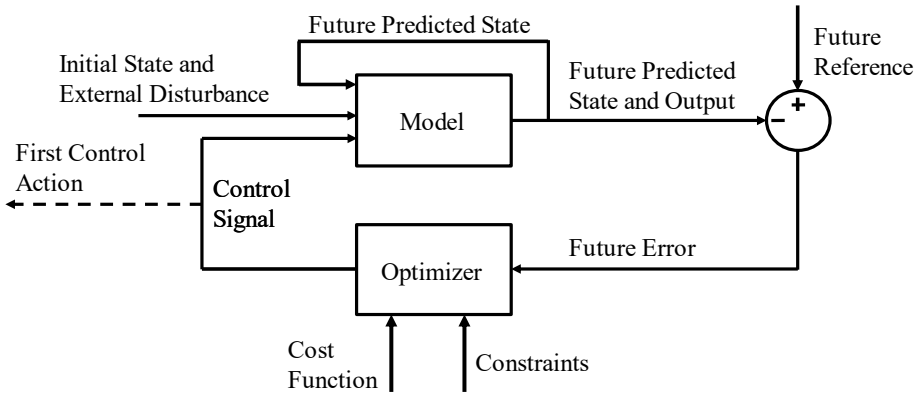

Figure 11: MPC block diagram

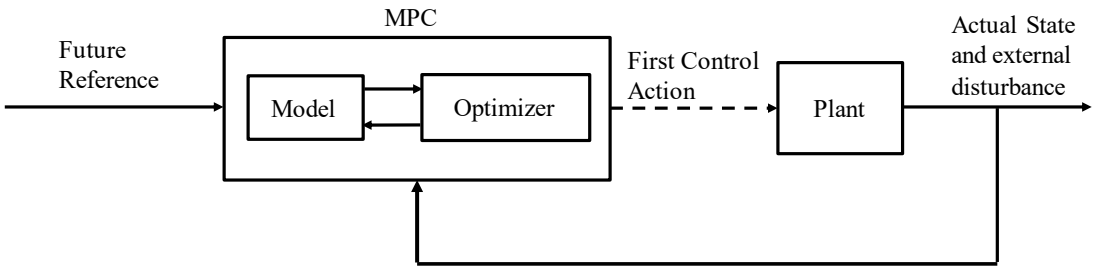

Figure 12: MPC linked with real system plant

The mathematical model of the A/C system for a conventional gasoline vehicle developed in Chapter 2 will be used by the MPC algorithm to predict the behaviour of the real system, taking the place of the model block in Figure 11 and Figure 12. At each timestep, an optimal sequence of control actions is computed by the MPC algorithm by running forecasts of the prediction model's behaviour in order to minimize the value of an objective function defined by the designer. An example of an objective function would be the error between a reference output trajectory and actual output trajectory for setpoint tracking, such as tracking an air temperature to a desired value. Once the optimal input sequence is computed, only the immediate next control action is sent to the real system and the response of the

system is fed back to the MPC. This behaviour adds robustness to the control because the MPC recomputes another optimal control sequence at each time step, whereas similar control approaches such as a linear quadratic regulator (LQR) computes an optimal control sequence offline for the entire simulation/cycle. At each time step, the MPC algorithm is reinitialized at the current operating condition of the system, that being the system state. If the behaviour of the real system is different than that predicted by the system model, this reinitialization compensates for those modelling errors and disturbances. At every subsequent timestep, a new optimal control sequence is computed, and this optimization window is shifted forward in time, one timestep each time. This is why MPC techniques are commonly referred to as receding horizon control [28].

As discussed in the literature review section, several linear approximation model predictive controllers have been formulated in the past, with the most popular being adaptive and gain-scheduled model predictive controllers [24], [25]. Figure 13 and Figure 14 depict block diagrams of these two MPC types.

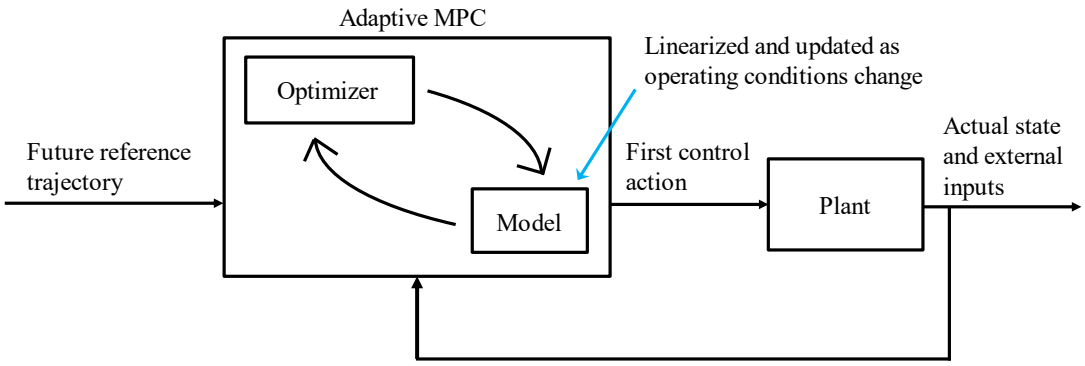

Figure 13: Adaptive MPC block diagram

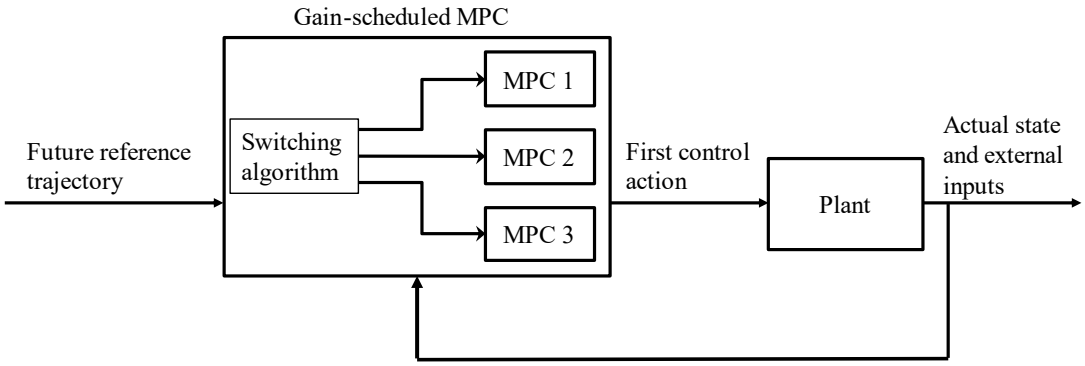

Figure 14: Gain-scheduled MPC block diagram

Both MPC types operate by finding multiple linearized models across the system's several operating points, but an adaptive model predictive controller type is better suited for this application. This is because the structure of the optimization problem (number of states and constraints) remains the same across different operating points, whereas gain-scheduled model predictive controllers are used when the number of states and constraints change between operating points. In the adaptive MPC, a linear model of the system is computed on the fly as the operating conditions are changing, and the internal prediction model is updated with each new linearized model. As the operating conditions are changing, only the model of the system is being updated, and the MPC algorithm stays the same. MPC strategies commonly use discrete state-space formulations for the mathematical modelling of the system of interest. The standard form of a discrete state-space system is written as:

$$\begin{aligned} x_{k+1} &= Ax_k + Bu_k + Ev_k \\ y_k &= Cx_k + Du_k + Fv_k \end{aligned} \tag{17}$$

where A, B, C, D, E, and F are matrices describing the linearized system dynamics, x_k is the state vector at timestep k, u_k is the controlled input vector at timestep k, v_k is the uncontrolled input vector at timestep k treated as an external disturbance, and y_k is the output vector at timestep k. As mentioned, the MPC computes an optimal input sequence using an optimizer and prediction model with the general form shown in (17). When looking at (17), it can be seen that when each control action is determined by the optimizer and sent to the discrete state-space model, the system state at the next timestep is calculated and the output at the current timestep is also determined. A forecast of future system state and output trajectories are computed using this discrete-time state-space prediction model.

As mentioned previously, the controller is designed in Simulink and is connected to the VEM model to create an SiL simulation environment. To achieve this, the controller code is compiled in Simulink to generate a C-code file that is executable by the VEM model in GT-Suite. The C-code file is embedded within the VEM model so that when the VEM model sends or receives signals from the controller, it is able to do so by executing the C-code file instead of requiring an external connection to Simulink.

3.3 Full Description of System Modelling, States, Inputs, and Outputs

As mentioned, the goal of this research is to develop an MPC that can reduce the energy consumption of the A/C system of a conventional gasoline vehicle. The cabin cooling effort of the A/C system is controlled using several actuators, three of which are the compressor clutch, condenser fan, and active grille shutters. These three controllable actuators, as well as other parameters, are displayed in a diagram of the A/C system shown in Figure 1. The compressor clutch connects the compressor to the engine, enabling the compressor to operate and increase the pressure of the refrigerant leaving through the discharge port. The condenser fan and AGS regulate the flow of the ambient air stream entering the front-end of the vehicle, which passes through the condenser to exchange heat with the refrigerant.

To define the aspects of the prediction model described by (17), the system of nonlinear equations described by (2) and (4) must be linearized. An additional equation is introduced to gather the individual power consumptions into one term, that being the total power consumption. The total power consumption of the A/C system is thus described by:

$$\dot{W}_{total} = \dot{W}_{comp} + \dot{W}_{fan} + \Delta\dot{W}_{drag} \tag{18}$$

These equations are linearized on the fly using the adaptive MPC approach described earlier, allowing the trim state to always be the current working state of the VEM model (real system). This allows the controller to be initialized at the current system state at each time step, allowing accuracy to be held throughout the simulation, since the controller will always be working in the vicinity of the trim state. To compute the linearization, the Jacobian matrices of the nonlinear model are evaluated at the current trim state, yielding the numeric values of the linearized system matrices.

The state vector x is described by (19):

$$x = \begin{bmatrix} p_c \\ p_e \end{bmatrix} = \begin{bmatrix} x_1 \\ x_2 \end{bmatrix} \tag{19}$$

where p_c and p_e are the condenser and evaporator refrigerant pressures. The input vector u is described by (20):

$$u = \begin{bmatrix} \pi_c \\ \widehat{N} \\ X \end{bmatrix} = \begin{bmatrix} u_1 \\ u_2 \\ u_3 \end{bmatrix} \tag{20}$$

where π_c is a continuous compressor clutch signal, $\widehat{N}$ is the normalized rotational speed of the condenser fan between zero and one, X is the open-fraction of the AGS between zero

and one. An important aspect of this input vector must be mentioned. For the real system, the compressor clutch acts as a discrete signal (a value of zero for disengaged or one for engaged). Since state-space models assume continuous variables, the compressor clutch input is determined as a continuous signal but is rounded to either zero or one when sent to the real system to ensure agreement with the physical behaviour of the system's actuators. This simplification is necessary, but it is a shortcoming in this work since the intended action of the controller is being overridden. A suggestion for future advancement of this research would be to exchange the discrete clutch actuation control with the continuous displacement control of a variable displacement compressor. The measured disturbance (uncontrolled) input vector v is described by (21):

$$v = \begin{bmatrix} \dot{m}_{ref} \\ Q_e \\ T_{air,in,c} \\ T_{air,in,e} \\ h_{in,c} \\ v \\ h_{in,comp} \end{bmatrix} = \begin{bmatrix} v_1 \\ v_2 \\ v_3 \\ v_4 \\ v_5 \\ v_6 \\ v_7 \end{bmatrix} \tag{21}$$

where $\dot{m}_{ref}$ is the mass flow rate of the refrigerant set by the compressor in GT-Suite, Q_e is the volume flow rate of the air set by the evaporator blower model in GT-Suite, $T_{air,in,c}$ and $T_{air,in,e}$ are the air temperatures entering the condenser and evaporator, $h_{in,c}$ is the inlet enthalpy for the condenser, v is the vehicle speed, and $h_{in,comp}$ is the inlet enthalpy for the compressor. All the measured disturbances are treated as uncontrolled inputs that are sent from the VEM model to the MPC. The output vector, y, is described by (22):

$$y = \begin{bmatrix} T_{air,out,e} \\ \dot{W}_{total} \end{bmatrix} = \begin{bmatrix} y_1 \\ y_2 \end{bmatrix} \tag{22}$$

where $T_{air,out,e}$ is the temperature of the air leaving the evaporator (entering the cabin), and $\dot{W}_{total}$ is the total power consumption of the compressor, $\dot{W}_{comp}$, fan, $\dot{W}_{fan}$, and additional power consumed due to underhood vehicle drag, $\Delta\dot{W}_{drag}$. The evaporator outlet air temperature is chosen as one of the outputs for the model because the goal of the controller is to control the actuators to maintain this air temperature close to a reference value, thus regulating the cabin cooling performance. The other output, $\dot{W}_{total}$, is chosen because the

second goal of this controller is to minimize the power consumption of the A/C system while satisfying the cooling objective.

Now that the underlying equations, states, inputs, and outputs have been clearly defined, the process of linearizing and discretizing the nonlinear equations described by (2), (4), and (18) can be discussed. The numerical values of the state-space matrices are computed using a successive linearization approach [29]. Successive linearization is a very popular approach adopted for adaptive MPC designs found in literature [30]. The concept of this approach is simple. At the beginning of each control iteration, the Jacobian matrices are evaluated at the current operating conditions of the complex system model, that being the current values for the system states, controlled inputs, and uncontrolled inputs. This will update the numerical values of the state-space matrix entries. By re-evaluating the state-space model at the current operating conditions, this will ensure that the trim state is close to the current operating point. The intention of this is to reduce the linearization error caused by deviations from the trim state. Thus, the working condition of the complex system model will be treated as the trim state.

The continuous-time linear state-space model form must be discretized to form a discrete-time linear state-space model. Typically, MPC algorithms are designed in discrete-time. An overwhelming amount of MPC designs have been developed using discrete-time approaches, and a much smaller amount of continuous-time MPCs are present in the literature. In this work, a discrete-time MPC has been chosen due to the nature of the communication between the MPC and the real system. The VEM model only communicates in discrete time steps, so to maintain consistency, the MPC has been designed in discrete-time as well. The discrete-time model was approximated from the continuous-time model using the forward Euler method, simply by multiplying the matrices by a constant time step of one second, as shown below [31]:

$$
\begin{aligned}
A &= I + A_c * T_s \\
B &= B_c * T_s \\
C &= C_c * T_s \\
D &= D_c * T_s \\
E &= E_c * T_s \\
F &= F_c * T_s
\end{aligned}
\tag{23}
$$

Where A_c, B_c. C_c. D_c, E_c, and F_c are the continuous-time state-space matrices, T_s is a constant time step, and I is an identity matrix. Normally, continuous-time state-space models are converted to discrete-time using MATLAB's built-in functions. However, due to limitations with functions supported by code generation in Simulink, the forward Euler approximation was adopted in this case. The discrete-time state-space matrices in this work are shown in (24). However, due to the nature of adaptive MPC, these system matrices are changing at each global time step, so the matrices in (24) are an example of state-space matrices at one specific operating condition.

$$
\begin{aligned}
A &= \begin{bmatrix} -0.0879 & 0 \\ 0.00224 & -0.154 \end{bmatrix} \\
B &= \begin{bmatrix} 39.4 & -53.3 & -40.9 \\ -16.8 & 0 & 0 \end{bmatrix} \\
C &= \begin{bmatrix} 0 & 0.104 \\ 0 & 0 \end{bmatrix} \\
D &= \begin{bmatrix} 0 & 0 & 0 \\ 0.992 & 0.331 & 0.0189 \end{bmatrix} \\
E &= \begin{bmatrix} 2000.03 & 0 & 3.29 & 0 & 0.237 & -0.914 & 0 \\ -850.5 & 62.8 & 0 & 1.18 & 0 & 0 & 0 \end{bmatrix} \\
F &= \begin{bmatrix} 0 & 0 & 0 & 0 & 0 & 0 & 0 \\ 50.3 & 0 & 0 & 0 & 0.0214 & -2.94e^{-5} & -0.0214 \end{bmatrix}
\end{aligned}
\tag{24}
$$

Using a time step of one second leaves only the A matrix changed, due to the addition of the identity matrix. The time step value used here is the same time step used in the optimal control iterative calculations, as well as the same time step used for communication between the VEM model and the MPC. A time step of one second was chosen as the value for this parameter. To validate the chosen time step, the time responses of the air temperature output were evaluated for a unit step from each of the three controlled inputs. The fastest time constant was found to be approximately 10.9 seconds, which was for the clutch unit step input. It is a common best practice for a discretization time step to be at least ten

times smaller than the fastest time constant of the system. Since the fastest time constant is 10.9 seconds, a discretization time step of one is satisfactory based on this best practice.

3.4 Quadratic Programming Formulation

Quadratic programming (QP) is an optimization process used to solve mathematical problems containing quadratic functions. This is the optimization technique used to determine the optimal input sequence needed to satisfy the objectives outlined for this research, which are temperature tracking and power consumption reduction. The optimal solution to a quadratic programming problem is found by minimizing the following objective function, J:

$$J = \min\left[\frac{1}{2}X_{qp}^{T}HX_{qp} + f^{T}X_{qp}\right] \tag{25}$$

where X_{qp} is a vector containing the control objectives shown in (26), H is a diagonal matrix containing relative weightings for each control objective in the quadratic term of the cost function, and f is a vector containing relative weightings for each control objective in the linear term of the cost function. Clearly, there is a quadratic term ($\frac{1}{2}X_{qp}^{T}HX_{qp}$) and a linear term ($f^{T}X_{qp}$) in the objective function. Adding the quadratic term is the difference between linear and quadratic problems. In this cost function, the elements of the vector X_{qp} are minimized to achieve the smallest possible value for the objective function. The X_{qp} vector is specific to a particular control problem being solved and can vary depending on what the objectives of the control are. For example, in state-space control, there are outputs, states, and inputs. For this control type, the controller is typically designed to track reference values for the states and outputs of the system, while also considering the magnitude and rate of change of the controlled input values. In this case, the elements of X_{qp} are as follows:

$$X_{qp} = \begin{bmatrix} y_k - y_{k,s} \\ x_k - x_{k,s} \\ u_k \\ \Delta u_k \end{bmatrix} \tag{26}$$

This description of X_{qp} is for a discrete time case, since the approach used for the controller design discussed in subsequent sections is also discrete time, due to the nature of the controller type. The first term, $y_k - y_{k,s}$, denotes the deviation between the current output value and the desired output reference value at time step k. The second term, $x_k - x_{k,s}$,

denotes the deviation between the current state value and the desired state reference value at time step k. The third term, u_k, denotes the magnitude of the controlled actuator inputs. This term is included to reduce the actuator effort in the control scheme. The fourth term, Δu_k, is added to X_{qp} to reduce the rate of change of the controlled actuator inputs from one control action to the next if chattering behaviour is a concern for the system of interest. Chattering behaviour is described as high-frequency oscillations of a controlled input, which can impact the durability of the controlled actuators. For this paper, all four of these elements are considered in the QP formulation. The elements along the diagonal of the *H* matrix can be used to change to relative importance of each control objective, even removing one completely from the problem by setting it's corresponding *H* matrix element to zero.

In order for the QP solver in MATLAB to know what the elements of the X_{qp} vector are, the elements of the X_{qp} vector must appear explicitly in the system of equations, the discrete state-space model in this case. The X_{qp} vector can be defined mathematically by reorganizing the state-space formulation described by (17) to explicitly include the elements of (26). Firstly, the model in (17) is rewritten as:

$$\begin{aligned} x_{k+1} &= Ax_k + B\Delta u_k + Bu_{k-1} \\ u_k &= u_{k-1} + \Delta u_k \\ y_k &= Cx_k + D\Delta u_k + Du_{k-1} \end{aligned} \tag{27}$$

where $\Delta u_k \triangleq u_k - u_{k-1}$. Rewriting the model in this form incorporates the rate of change of the controller inputs into the state-space model. The next step is to rewrite the state-space model in terms of setpoint deviations. This model is shown in (28):

$$\begin{aligned} x_{k+1} - x_{k+1,s} &= A\big(x_k - x_{k,s}\big) + Ax_{k,s} + B\Delta u_k + Bu_{k-1} - x_{k+1,s} \\ u_k &= u_{k-1} + \Delta u_k \\ y_k - y_{k,s} &= C\big(x_k - x_{k,s}\big) + Cx_{k,s} + D\Delta u_k + Du_{k-1} - y_{k,s} \end{aligned} \tag{28}$$

where the subscript s denotes a setpoint. Based on the formulation above, setpoints must be set for the states and outputs. The setpoints for the states are set as the trim state to ensure the heat exchanger pressures remain within typical operating conditions. As will be discussed later, the weighting for the state error will be given a small importance relative to the main control objectives for this work, such as the error for the air temperature sent

to the cabin. The setpoint for the air temperature sent to the cabin is 4°C, which is set by the industrial partner. Since the power consumption must be reduced, the setpoint for the power is set as zero.

To simplify the presentation of the equations shown in (28), the following variable definitions are introduced:

$$\begin{gathered} x'_k = \begin{bmatrix} x_k - x_{k,s} \\ u_{k-1} \end{bmatrix} \\ A' = \begin{bmatrix} A & B \\ 0_{n_u \times n_x} & I_{n_u \times n_u} \end{bmatrix} \\ B' = \begin{bmatrix} B \\ I_{n_u \times n_u} \end{bmatrix} \\ x'_{k,s} = \begin{bmatrix} x_{k,s} \\ 0_{n_u \times 1} \end{bmatrix} \\ y'_k = y_k - y_{k,s} \\ C' = \begin{bmatrix} C & D \end{bmatrix} \end{gathered} \tag{29}$$

resulting in the final form equations shown in (30):

$$\begin{gathered} x'_{k+1} = A'x'_k + B'\Delta u_k - x'_{k+1,s} + A'x'_{k,s} \\ y'_k = C'x'_k + D\Delta u_k - y_{k,s} + C'x'_{k,s} \end{gathered} \tag{30}$$

Now it can be seen that the four elements of X_{qp} appear explicitly in the state-space model. To be clear, the model shown in (30) is not the internal prediction model used to determine the system behaviour when acted upon by the optimal input sequence computed by the MPC. The model in (30) is created to allow the QP solver to understand what must be minimized, that being the elements of X_{qp}. In QP problems, the elements of the X_{qp} vector are defined by rearranging the system equations to form an equality constraint of the form $Ax = b$. The elements in the A matrix on the left-hand side of the equality are multiplied by the elements of x, which is X_{qp} in this case. This means terms on the left-hand side of the equality must be the terms in (30) that contain elements of X_{qp}. The elements in the b vector on the right-hand side of the equality are the remaining terms, which turn out to be setpoint deviations.

To achieve this form, the model shown in (30) can be rearranged in the following form:

$$\begin{aligned} x'_{k+1} - A'x'_k - B'\Delta u_k &= A'x'_{k,s} - x'_{k+1,s} \\ y'_k - C'x'_k - D\Delta u_k &= -y_{k,s} + C'x'_{k,s} \end{aligned} \tag{31}$$

The equations shown in (31) are of the form:

$$A_{eq}X_{qp} = b_{eq} \tag{32}$$

where X_{qp}, A_{eq}, and b_{eq} are defined as:

$$X_{qp} = \begin{bmatrix} x'_k \\ \Delta u_k \\ x'_{k+1} \\ y'_k \end{bmatrix} \tag{33}$$

$$A_{eq} = \begin{bmatrix} -A' & -B' & I_{n_{x'}} & 0 \\ -C' & -D' & 0 & I_{n_y} \end{bmatrix} \tag{34}$$

$$b_{eq} = \begin{bmatrix} A'x'_{k,s} - x'_{k+1,s} \\ -y_{k,s} + C'x'_{k,s} \end{bmatrix} \tag{35}$$

The matrices in equations (33)-(35) are for a single control interval. As mentioned earlier, MPC run the model forward in time in a series of forecasts to predict the future behaviour of the system. The length in which this is done is called the prediction horizon, denoted as h, which is the number of control intervals, measured in discrete time steps, the model is forecasted ahead in time. The length of the matrices in equations (33)-(35) are dependent upon the length of the prediction horizon. The general form of the matrices are:

$$X_{qp} = \begin{bmatrix} \Delta u_0 \\ x'_1 \\ \vdots \\ \Delta u_{h-1} \\ x'_h \\ y'_1 \\ \vdots \\ y'_h \end{bmatrix}_{1\times h(n_x+2n_u+n_y)} \tag{36}$$

$$A_{eq} = \begin{bmatrix} -B' & I_{n_{x'}} & 0 & 0 & \cdots & \cdots & \cdots & \cdots & 0 \\ 0 & -A' & -B' & I_{n_{x'}} & \ddots & \ddots & \ddots & \ddots & \vdots \\ \vdots & \ddots & \ddots & \ddots & \ddots & \ddots & \ddots & \ddots & \vdots \\ 0 & \cdots & 0 & -A' & -B' & I_{n_{x'}} & 0 & \cdots & 0 \\ -D & -C' & \cdots & \cdots & \cdots & 0 & I_{n_y} & \cdots & 0 \\ \vdots & \ddots & \ddots & \ddots & \ddots & \ddots & \ddots & \ddots & 0 \\ 0 & \cdots & \cdots & \cdots & -D & -C' & \cdots & 0 & I_{n_y} \end{bmatrix}_{h(n_x+n_u+n_y)\times h(n_x+2n_u+n_y)} \tag{37}$$

$$b_{eq} = \begin{bmatrix} A'\begin{bmatrix} x_0 \\ u_{-1} \end{bmatrix} - x'_{1,s} \\ A'x'_{1,s} - x'_{2,s} \\ \vdots \\ A'x'_{h-1,s} - x'_{h,s} \\ -y_{0,s} + C'x'_{0,s} \\ \vdots \\ -y_{h,s} + C'x'_{h,s} \end{bmatrix}_{h(n_x+n_u+n_y)\times 1} \tag{38}$$

where n_x is the number of states, n_u is the number of controlled, n_y is the number of outputs. At each time step, the controller undergoes a number of optimizations (minimizations of the X_{qp} vector) equal to the length of the prediction horizon. For example, if the prediction horizon is equal to ten discrete time steps, the controller will minimize X_{qp} at the initial time step, apply the optimal control input to the prediction plant model, measure the response from the prediction model, then use the response to calculate the next control input. This process is repeated nine more times in this case, with X_{qp} being minimized at each control step. In this example, if the total simulation time is 100 seconds, the MPC will be run 1000 times since it computes ten optimal input actions at each time step. The prediction horizon length is a tunable parameter that is defined prior to solving the optimization problem. If the prediction horizon too short, it will not be able to cover the significant dynamics of the system. If a disturbance is applied to the system, it may not be able to react fast enough with a prediction horizon that is too short. If the prediction horizon is too long and a disturbance occurs, it could cause a large portion of the control prediction to be thrown away and recomputed to account for the disturbance. It is also more computationally expensive to have a large prediction horizon since the matrices become much larger and the MPC must compute more control actions over a larger optimization window.

A typical recommendation for MPC designs is to have the prediction horizon cover a significant portion of the transient open-loop system response, with 10-20 samples within that prediction horizon. The fastest time response of the system is roughly 21 seconds. Since the time step is one second, this means a prediction horizon of 21 samples would cover the entire transient portion of the open-loop system response. Due to a time-limitation on this work, the prediction horizon length was made to be 10 samples, since longer prediction horizons would warrant a significantly longer simulation time, which was not feasible given the timeline of this work. In future work for this project, longer prediction

horizons can be analyzed to investigate the tradeoff between computation time and model response.

The robustness of MPC can be clearly understood by this receding horizon behaviour. When the controller sends the immediate next control action to the complex system model, the expected response may differ from the actual response due to several factors such as linearization error or unmeasured disturbances. Instead of this error compounding over time, the controller can make corrections since an entirely new control sequence is computed at each time step. Although, this makes MPC very computationally expensive since a new optimal control problem is solved at each time step.

Constraints can be set on the optimization. The controlled inputs have physical limitations based on their range of operation. These are hard constraints that cannot be exceed by any means. The states also have constraints, but they are not due to physical limitations. The constraints on the states are imposed to prevent problems from arising in the HEXs due to excessive pressure or lack of pressure. For the QP algorithm to run successfully, constraints must also be present for the outputs as well, but since the outputs do not have bounds for this application, they will be treated as infinity. The constraints are shown in (39) and are defined by the industrial partner:

$$\begin{aligned} 100kPa \leq p_e \leq 1300kPa \\ 700kPa \leq p_c \leq 3000kPa \\ \pi_c = [0,1] \\ 0 \leq \widehat{N} \leq 1 \\ 0 \leq X \leq 1 \end{aligned} \tag{39}$$

Recall that the $\widehat{N}$ is the normalized rotational speed of the condenser fan, meaning a value of one indicates the maximum physical rotational speed. The same goes for X, the open fraction of the AGS, where a value of one indicates the fully open position. For quadratic programming in MATLAB, the upper and lower bounds for the constraints can be organized for the entire length of the prediction horizon in the form:

$$lb = \begin{bmatrix} lb_u - ub_u \\ \begin{bmatrix} lb_x - x_{1,s} \\ lb_u \end{bmatrix} \\ \vdots \\ lb_u - ub_u \\ \begin{bmatrix} lb_x - x_{h,s} \\ lb_u \end{bmatrix} \\ lb_y - y_{1,s} \\ \vdots \\ lb_y - y_{h,s} \end{bmatrix}_{h(n_x+n_u+n_y)\times 1} \tag{40}$$

$$ub = \begin{bmatrix} ub_u - lb_u \\ \begin{bmatrix} ub_x - x_{1,s} \\ ub_u \end{bmatrix} \\ \vdots \\ ub_u - lb_u \\ \begin{bmatrix} ub_x - x_{h,s} \\ ub_u \end{bmatrix} \\ ub_y - y_{1,s} \\ \vdots \\ ub_y - y_{h,s} \end{bmatrix}_{h(n_x+n_u+n_y)\times 1} \tag{41}$$

where lb_u and ub_u are the lower and upper bounds on the inputs, lb_x and ub_x are the lower and upper bounds on the states, and lb_y and ub_y are the lower and upper bounds on the outputs.

Each element of the X_{qp} vector can be weighted individually, providing more significance to the prioritization of certain control objectives over the others. The weighting matrix for the control objectives within the objective function (output reference tracking, state reference tracking, input value magnitude, and rate of change of the input commands) is shown below:

$$H = \begin{bmatrix} \begin{bmatrix} R_{\Delta u} & 0 \\ 0 & Q_x' \end{bmatrix} & 0 & \cdots & \cdots & \cdots & 0 \\ 0 & \ddots & \ddots & \ddots & \ddots & \vdots \\ \vdots & \ddots & \begin{bmatrix} R_{\Delta u} & 0 \\ 0 & Q_x' \end{bmatrix} & 0 & \cdots & 0 \\ 0 & \cdots & 0 & Q_y & \cdots & 0 \\ \vdots & \ddots & \ddots & \ddots & \ddots & \vdots \\ 0 & \cdots & \cdots & \cdots & 0 & Q_y \end{bmatrix}_{h(n_x+2n_u+n_y)\times h(n_x+2n_u+n_y)} \tag{42}$$

$$Q'_x = \begin{bmatrix} Q_x & 0_{n_x \times n_u} \\ 0_{n_u \times n_x} & R_u \end{bmatrix}_{(n_x+n_u)\times(n_x+n_u)}$$

where $R_{\Delta u}$ is the weighting of the rate of change of the inputs, Q_x is the weighting of the state reference tracking deviations, R_u is the weighting of the input magnitudes, and Q_y is the weighting of the output reference tracking deviations. $R_{\Delta u}$, Q_x, R_u, and Q_y are diagonal matrices with the respective weights along the diagonal. For example, this problem has two states, so the Q_x matrix is a 2x2 matrix with the value in position (1,1) pertaining to the first state deviation and the value in position (2,2) pertaining to the second state deviation. The variable names given to the individual weighting parameters are presented in equation (43).

$$\begin{aligned} Q_x &= \begin{bmatrix} K_{p_c} & 0 \\ 0 & K_{p_e} \end{bmatrix} \\ Q_y &= \begin{bmatrix} K_{T_{air}} & 0 \\ 0 & K_{\dot{W}_T} \end{bmatrix} \\ R_u &= \begin{bmatrix} K_{\pi_c} & 0 & 0 \\ 0 & K_{\widehat{N}} & 0 \\ 0 & 0 & K_X \end{bmatrix} \\ R_{du} &= \begin{bmatrix} K_{\Delta\pi_c} & 0 & 0 \\ 0 & K_{\Delta\widehat{N}} & 0 \\ 0 & 0 & K_{\Delta X} \end{bmatrix} \end{aligned} \tag{43}$$

where K_{p_c} is the weighting for the condenser pressure setpoint deviation, K_{p_e} is the weighting for the evaporator pressure setpoint deviation, $K_{T_{air}}$ is the weighting for the air temperature setpoint deviation, $K_{\dot{W}_T}$ is the weighting for the total power consumption, K_{π_c} is the weighting for the compressor clutch input absolute value, $K_{\widehat{N}}$ is the weighting for the normalized fan rotational speed input absolute value, K_X is the weighting for the AGS open-fraction input absolute value, $K_{\Delta\pi_c}$ is the weighting for the rate of change of the compressor clutch input, $K_{\Delta\widehat{N}}$ is the weighting for the rate of change of the normalized fan rotational speed input, and $K_{\Delta X}$ is the weighting for the rate of change of the AGS open-fraction input. The specific values for these weights will be discussed in section 3.5.

3.5 Results and Discussion

As mentioned previously, the controller is designed in Simulink and is connected to the VEM model to create an SiL simulation environment. To achieve this, the controller code is compiled in Simulink to generate a C-code file that is executable by the VEM model in GT-Suite. The C-code file is embedded within the VEM model so that when the VEM model sends/receives signals to/from the controller, it is able to do so by executing the C-code file instead of requiring an external connection to Simulink. This allows the MPC to be imbedded within the VEM model, meaning once the C-code file is received, the only software needed to simulate the controlled system is GT-Suite.

The main tunable aspects of the MPC controller are the weighting factors set for the individual elements of the objective function, defined in equation (33). Although there are weighting factors given to all elements of equation (33), some elements are clearly more important than others based on the problem definition for this work. The most crucial aspects of equation (33) to be minimized are: the air temperature setpoint deviation, the instantaneous power consumption, and the clutch actuation frequency. The air temperature setpoint deviation must be minimized, as this is the metric that governs the main goal of the A/C system, to send the correct air temperature to the cabin. The power consumption must be minimized due to the nature of the problem definition requested by the industrial partner. Finally, the clutch actuations are an important aspect to consider since the durability of the compressor can be a concern if a jittering phenomenon occurs, where the compressor clutch is constantly cycled between engaging and disengaging. Wear and tear on the compressor clutch can lead to reliability issues within vehicles and can increase expenses if the compressor requires maintenance more frequently. With these three weightings being identified as the crucial weightings of interest for the MPC tuning, all other weightings are set to a value of one, while the other three are varied, to ensure all aspects of the objective function are still being considered.

A preliminary sensitivity assessment was conducted to determine the search space ranges for these three weighting values to ensure the entire relevant search space is being explored. For the three main weightings, each individual weighting factor was systematically increased in value while all other weighting factors are held constant at a value of

one. For example, the weighting for the rate of change of the clutch engagement was increased until no further significant change was observed in the number of clutch actuations in the system. Table 5 shows the sensitivity analysis results.

Table 5: Weighting sensitivity analysis results

$K_{\Delta\pi_c}$ **Weight Value**	**1**	**10**	**100**	**500**	**1000**	**10000**
$\Delta\pi_c$ **Count**	152	116	16	2	0	0
$K_{T_{air}}$ **Weight Value**	**1**	**10**	**50**	**500**	**5000**	**50000**
T_{air} **RMSE**	4.59	4.51	4.47	4.47	4.48	4.46
$K_{\dot{W}_T}$ **Weight Value**	**1**	**10**	**50**	**100**	**1000**	**10000**
$\dot{W}_T$	943.1	872.3	798.0	20.3	20.2	20.2

The valid weighting ranges for $K_{\Delta\pi_c}$ has been identified as 1 – 1000, since values greater than 1000 present no change to the number of clutch actuations. The valid weighting range for $K_{T_{air}}$ is between 1 – 50, as these values above this range provide no significant change to the air temperature RMSE. Finally, the valid weighting range for $K_{\dot{W}_T}$ is chosen to be between 1 – 50, since values greater than 50 cause the compressor to shut off completely for the entire cycle, meaning the A/C system is unactive and the air temperature RMSE reaches extreme, unrealistic values. The effective weighting range for $K_{\Delta\pi_c}$ holds values much greater than that of $K_{T_{air}}$ and $K_{\dot{W}_T}$, since the value of the clutch rate of change can only ever be between zero and one, whereas the values of the air temperature RMSE and power consumption are greater, namely around 4°C and 4kW.

A Latin Hypercube Sampling (LHS) approach was used to determine the investigated values for the three main MPC weightings within the defined search spaces [32]. A sample space of 200 unique combinations of weighting values were randomly generated in MATLAB using LHS to adequately fill the search space defined earlier. The LHS search space is shown in Figure 15.

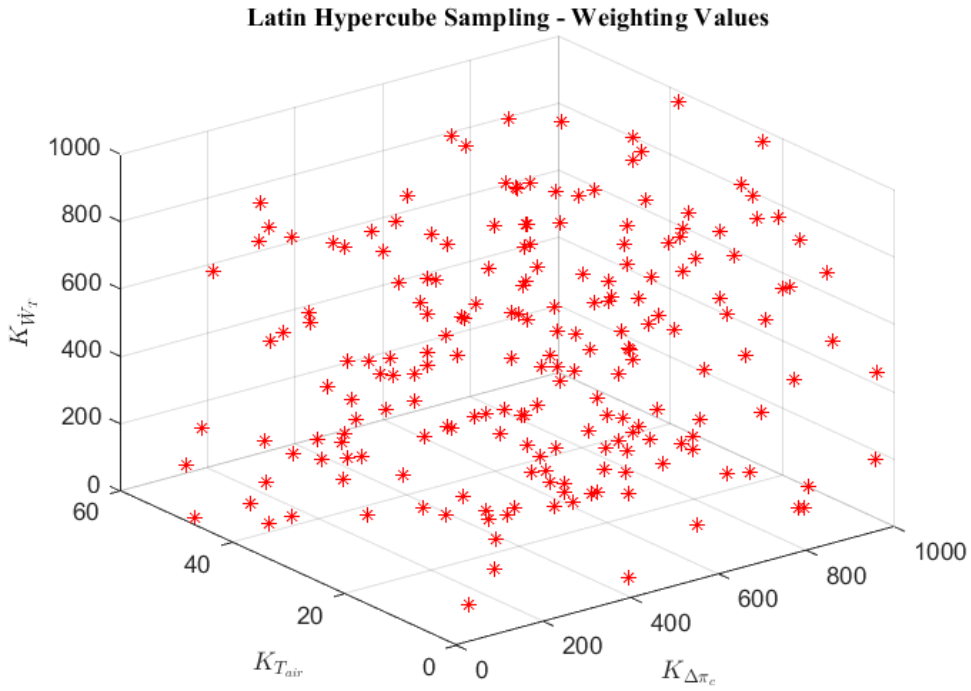

Figure 15: LHS sample space search

The performance of the VEM model with the baseline control scheme is restated here in Table 6, where $n_{\Delta\pi_c}$ is the number of clutch actuations. These metrics will be referenced to the MPC results to compare the improvement of the new control scheme.

Table 6: Baseline VEM model performance metrics

Model	T_{eao} ***RMSE*** **[C]**	$\dot{W}_T$ **[kJ]**	$n_{\Delta\pi_c}$
Baseline VEM	6.27	1262.8	0

The MPC was simulated with the VEM model for each set of 200 weighting combinations to assess the behaviour of the system with the new control scheme. As stated earlier, the three main metrics of interest are the RMSE for the air temperature setpoint deviation, the total energy consumption throughout the entire cycle, and the total number of clutch actuations. The VEM model was simulated for the SC03 drive cycle, and the results are plotted in Figure 16.

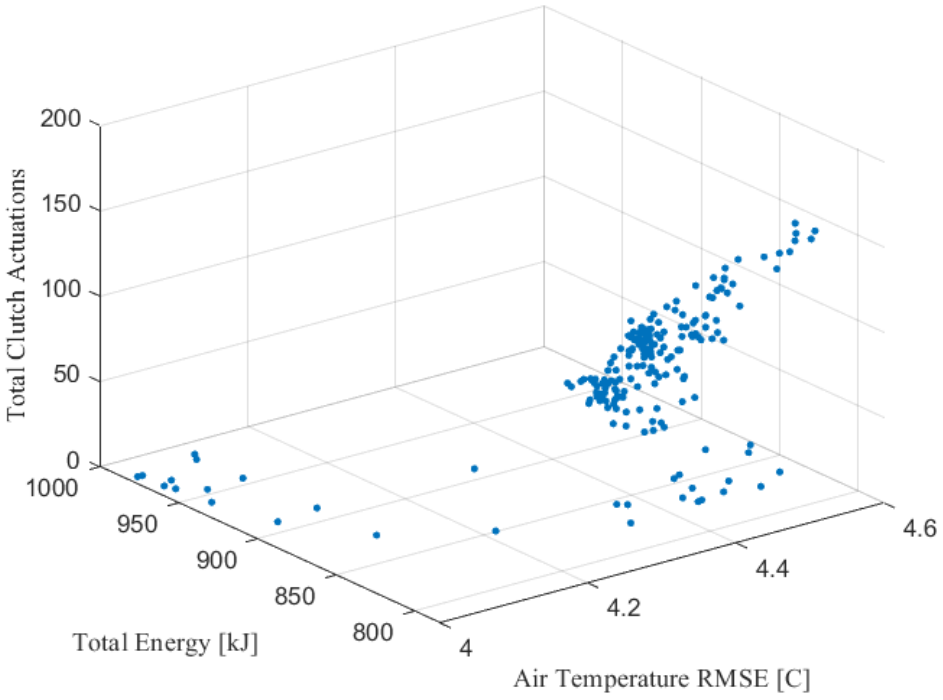

Figure 16: Evaluation of MPC control of VEM model for SC03 drive cycle

To get a clearer picture of the distribution of the results, the 2-D side profiles of each view are plotted in Figure 17 – Figure 19, with the depth being represented by a color bar encompassing the values of the third variable in each case.

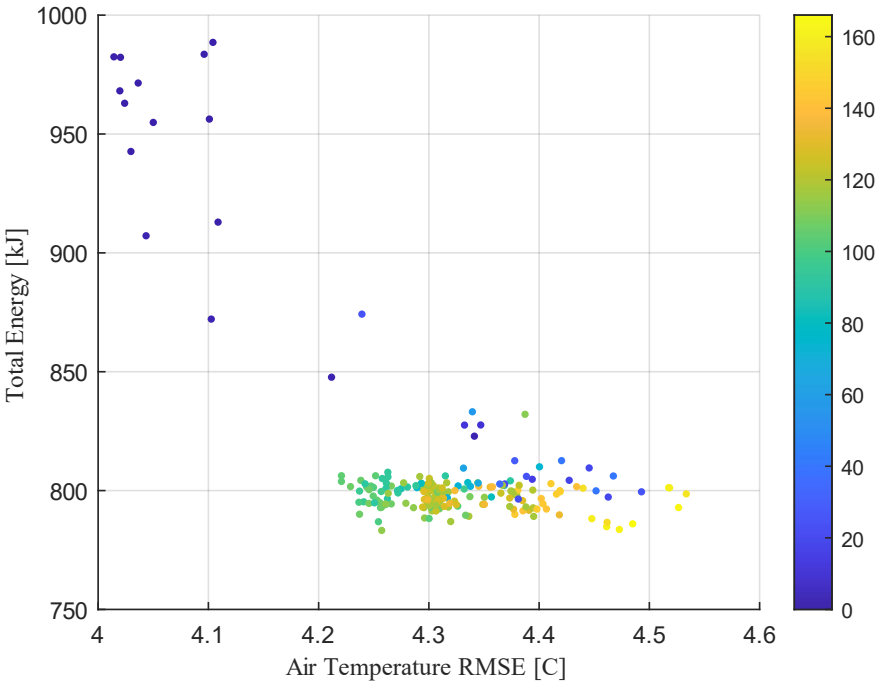

Figure 17: Air temperature RMSE vs total energy profile for MPC results

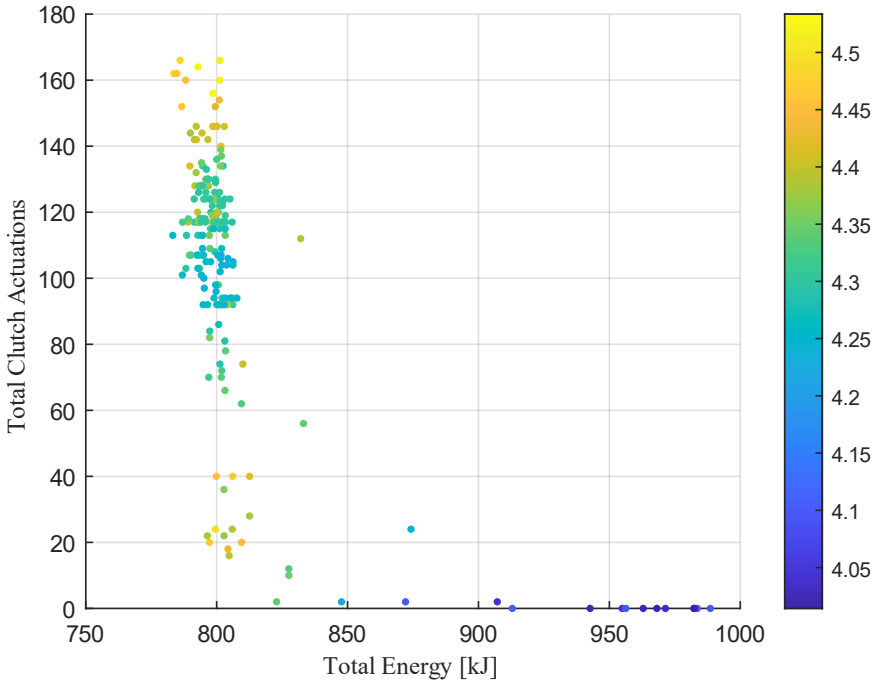

Figure 18: Total energy vs total clutch actuations profile for MPC results

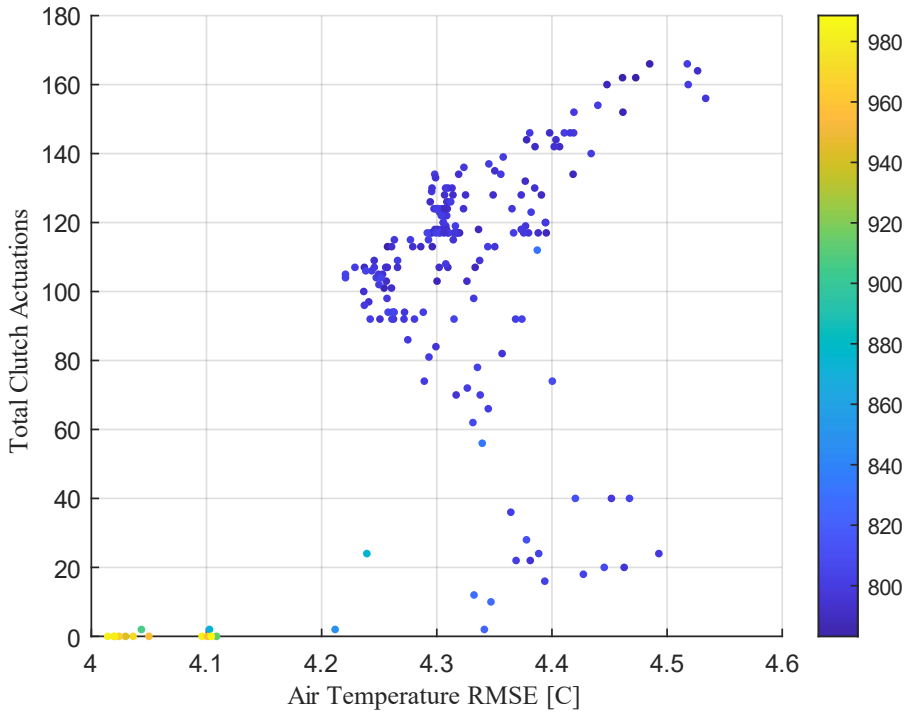

Figure 19: Air temperature RMSE vs total clutch actuations profile for MPC results

The trade-offs between the three output metrics can be observed through these figures. Figure 17 and Figure 18 demonstrate that the number of clutch actuations strongly impacts the air temperature RMSE and the total energy consumption of the A/C system. Some points of interest (POI) from the MPC results shown in Figure 17 – Figure 19 are gathered in Table 7. When the clutch does not actuate in POI 1, the energy consumption is at its highest, however, the air temperature RMSE is at its lowest. This scenario is most similar to the baseline control since the built-in compressor displacement control is the main driving force for the refrigerant control. Since the compressor is active during the entire cycle in this case, the energy consumption is high, since the compressor is the main energy consumer for the A/C system, as seen in Figure 8. Comparing this POI with the baseline VEM control scheme performance, the energy consumption is reduced by 20.9% and the air temperature RMSE is reduced by 34.6%. This demonstrates that by just using MPC control of the compressor, fan and, AGS, there is significant improvement to the reference temperature tracking and energy consumption.

An interesting impact can be observed by increasing the compressor clutch actuations by a small margin, from POI 1 to POI 2 and 3, which is done by decreasing the weighting value of $K_{\Delta\pi_c}$ or increasing the weighting values of $K_{T_{air}}$ and $K_{\dot{W}_T}$. By increasing the actuations from zero to two, the energy consumption is decreased by 30.9% compared to the baseline. Similarly from zero to ten actuations, the energy consumption is reduced by 34.5% compared to the baseline. However, the RMSE for the air temperature is increased from 4.10°C to 4.35°C.

Figure 19 demonstrates that when the compressor clutch actuations are above 20, no significant improvement to the energy consumption is achieved. Although, in this region, the best air temperature RMSE is found between roughly 95 – 110 clutch actuations.

Table 7: MPC results comparison to baseline controls performance

Model	T_{eao} **RMSE [C]**	$\dot{W}_T$ **[kJ]**	$n_{\Delta\pi_c}$
Baseline VEM	6.27	1262.8	0
POI 1	4.10	998.6	0
POI 2	4.10	872.1	2
POI 3	4.35	827.6	10
POI 4	4.46	797.3	20
POI 5	4.22	797.0	105
POI 6	4.44	788.2	160

The main outcome of this analysis is to show that there are several interesting operating regions for MPC designs depending on the objective importance preferred by the designer. Energy consumption reduction is normally of the highest importance for production vehicles, so increasing the compressor clutch actuations shows a clear improvement at the expense of less clutch durability. By increasing the amount of clutch actuations further, the air temperature RMSE can be reduced to roughly 4.2°C. However, if a small sacrifice in air temperature RMSE is accepted, namely increasing it to roughly 4.4°C, the clutch durability can be improved by reducing the actuations from 105 down to 20.

Figure 20 shows the air temperature reference tracking for POI 5. It is clear that the MPC is able to track to the reference temperature, but due to the discrete nature of the clutch, a steady-state response is not able to be achieved in this way. The steep spikes in the response are due to the cycling of the clutch on/off. When the clutch is engaged, the

temperature slowly declines. Once the temperature falls too far below the setpoint, the clutch is disengaged for a short period of time to allow the air temperature to increase before engaging the clutch once more.

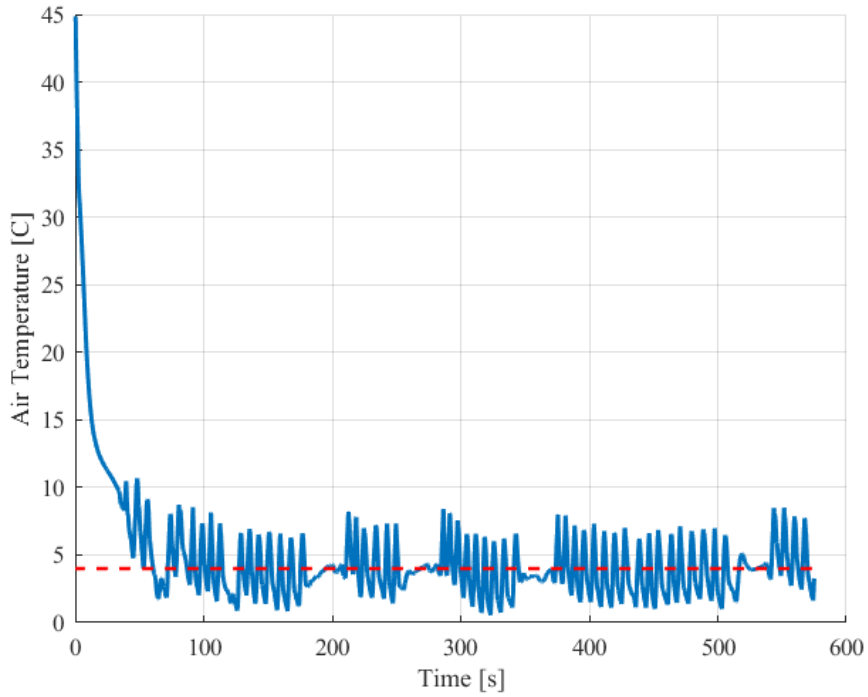

Figure 20: Air temperature output tracking for POI 5

3.6 Conclusions and Future Works

The analysis in this work shows that by switching to MPC control, a significant improvement to the air temperature reference tracking and energy consumption can be achieved. By disengaging the compressor when it is not needed, a significant amount of energy savings is recorded, however, achieving a steady-state solution at the air temperature setpoint of 4°C was not achievable by controlling the fan and AGS alone, leading to a cycling behaviour of the discrete compressor clutch. By slightly increasing the number of actuations made by the compressor clutch, a significant energy benefit is observed, but no further energy benefit is observed by increasing the clutch actuations further. However, a positive impact on the air temperature RMSE is seen by increasing the clutch actuations from 20 to 105, at the expense of more wear and tear on the clutch itself.

As seen in the results presented, a major shortcoming in this work with regards to the air temperature RMSE was the control of a discrete compressor clutch. The continuous input action desired by the MPC was being overridden for the clutch signal since the clutch is discrete in nature. The control of the clutch lead to a heavily transient response with the air temperature sent to the cabin. When the clutch is engaged, the air temperature slowly decreases until it is too far below the setpoint, after which the compressor clutch disengages and the temperature spikes back up. This causes aggressive actuation of the compressor clutch when the weighting for the air temperature reference error is high, and the controller will never be able to reach a smooth response. To improve upon this, the displacement of the compressor should be controlled instead. By controlling the displacement of the compressor, a smoother response can be achieved since the displacement is a continuous variable, unlike the compressor clutch. This means the control action computed by the MPC will not be overridden and the response of the system will be closer to what the controller expects. This will also prevent durability issues with the frequent on/off cycling of the compressor clutch.

REFERENCES

[1] Gamma Technologies, "GT-SUITE," *GT-Suite Integrated Multi-physics Systems Simulation*. https://www.gtisoft.com/gt-suite/ (accessed Nov. 23, 2022).

[2] Q. Zhang, "Modeling, Energy Optimization and Control of Vapor Compression Refrigeration Systems for Automotive Applications," The Ohio State University, 2014. Accessed: Apr. 24, 2022. [Online]. Available: https://etd.ohiolink.edu/apex-prod/rws_olink/r/1501/10?clear=10&p10_accession_num=osu1406121484

[3] Y. A. Çengel and M. Boles, *Thermodynamics: An Engineering Approach*, Ninth Edition. Boston: McGraw-Hill Higher Education, 2019.

[4] J. P. Boyd, "Six strategies for defeating the Runge Phenomenon in Gaussian radial basis functions on a finite interval," *Comput. Math. Appl.*, vol. 60, no. 12, pp. 3108–3122, Dec. 2010, doi: 10.1016/j.camwa.2010.10.015.

[5] S. L. Dixon and C. A. Hall, *Fluid mechanics and thermodynamics of turbomachinery*, Seventh edition. Amsterdam ; Boston: Butterworth-Heinemann is an imprint of Elsevier, 2014.

[6] Y. Huang, A. Khajepour, M. Khazraee, and M. Bahrami, "A Comparative Study of the Energy-Saving Controllers for Automotive Air-Conditioning/Refrigeration Systems," *J. Dyn. Syst. Meas. Control*, vol. 139, no. 1, Oct. 2016, doi: 10.1115/1.4034505.

[7] L. Chengguo, E. Brewer, L. Pham, and H. Jung, "Reducing Mobile Air Conditioner (MAC) Power Consumption Using Active Cabin-Air-Recirculation in A Plug-In Hybrid Electric Vehicle (PHEV)," *World Electr. Veh. J.*, vol. 9, p. 51, Dec. 2018, doi: 10.3390/wevj9040051.

[8] J. Liu, H. Zhou, X. Zhou, Y. Cao, and H. Zhao, "Automotive air conditioning system control - A survey," in *Proceedings of 2011 International Conference on Electronic & Mechanical Engineering and Information Technology*, Aug. 2011, pp. 3408–3412. doi: 10.1109/EMEIT.2011.6023817.

[9] Y. Xie *et al.*, "A Self-learning intelligent passenger vehicle comfort cooling system control strategy," *Appl. Therm. Eng.*, vol. 166, p. 114646, Feb. 2020, doi: 10.1016/j.applthermaleng.2019.114646.

[10] G. Høgh and R. Nielsen, "Model Based Nonlinear Control of Refrigeration Systems," Aalborg University, 2008.

[11] I. Cvok, B. Škugor, and J. Deur, "Control trajectory optimisation and optimal control of an electric vehicle HVAC system for favourable efficiency and thermal comfort," *Optim. Eng.*, pp. 1–13, 2020, doi: 10.1007/s11081-020-09515-w.

[12] B. Koo, Y. Yoo, and S. Won, "Super-twisting algorithm-based sliding mode controller for a refrigeration system," in *2012 12th International Conference on Control, Automation and Systems*, 2012, pp. 34–38.

[13] N. Kim *et al.*, "Robust Sliding Mode Control of a Vapor Compression Cycle," *Int. J. Control Autom. Syst.*, vol. 16, no. 1, pp. 62–78, 2018, doi: 10.1007/s12555-016-0584-7.

[14] Y. Huang, A. Khajepour, H. Ding, F. Bagheri, and M. Bahrami, "An energy-saving set-point optimizer with a sliding mode controller for automotive air-conditioning/refrigeration systems," *Appl. Energy*, vol. 188, pp. 576–585, 2017, doi: 10.1016/j.apenergy.2016.12.033.

[15] S. Borreggine, V. G. Monopoli, G. Rizzello, D. Naso, F. Cupertino, and R. Consoletti, "A Review on Model Predictive Control and its Applications in Power Electronics," in *2019 AEIT International Conference of Electrical and Electronic Technologies for Automotive (AEIT AUTOMOTIVE)*, Jul. 2019, pp. 1–6. doi: 10.23919/EETA.2019.8804594.

[16] V. Havlena and P. Barva, "Model Predictive Control - Review and Case Study," *IFAC Proc. Vol.*, vol. 33, no. 13, pp. 233–238, 2000, doi: 10.1016/s1474-6670(17)37195-1.

[17] L. F. S. Larsen, T. Geyer, and M. Morari, "Hybrid {MPC} in Supermarket Refrigeration Systems," *Proc 16th IFAC World Congr.*, no. October 2005, 2005.

[18] D. Sarabia, F. Capraro, L. F. S. Larsen, and C. De Prada, "Hybrid control of a supermarket refrigeration systems," *Proc. Am. Control Conf.*, no. August, pp. 4178–4185, 2007, doi: 10.1109/ACC.2007.4282661.

[19] C. Sonntag, A. Devanathan, S. Engell, and O. Stursberg, "Hybrid Nonlinear Model-Predictive Control of a Supermarket Refrigeration System," in *2007 IEEE International Conference on Control Applications*, Oct. 2007, pp. 1432–1437. doi: 10.1109/CCA.2007.4389437.

[20] Y. Huang, H. Wang, A. Khajepour, H. He, and J. Ji, "Model predictive control power management strategies for HEVs: A review," *J. Power Sources*, vol. 341, pp. 91–106, 2017, doi: 10.1016/j.jpowsour.2016.11.106.

[21] H. Wang *et al.*, "MPC-based Precision Cooling Strategy (PCS) for Efficient Thermal Management of Automotive Air Conditioning System," in *2019 IEEE Conference on Control Technology and Applications (CCTA)*, Aug. 2019. doi: 10.1109/CCTA.2019.8920526.

[22] S. Schaut and O. Sawodny, "Thermal Management for the Cabin of a Battery Electric Vehicle Considering Passengers' Comfort," *IEEE Trans. Control Syst. Technol.*, vol. 28, no. 4, pp. 1476–1492, 2020, doi: 10.1109/TCST.2019.2914888.

[23] H. Wang, I. Kolmanovsky, M. R. Amini, and J. Sun, "Model Predictive Climate Control of Connected and Automated Vehicles for Improved Energy Efficiency," in *Proceedings of the American Control Conference*, Aug. 2018, vol. 2018-June, pp. 828–833. doi: 10.23919/ACC.2018.8431051.

[24] V. Adetola, D. DeHaan, and M. Guay, "Adaptive model predictive control for constrained nonlinear systems," *Syst. Control Lett.*, vol. 58, no. 5, pp. 320–326, 2009, doi: 10.1016/j.sysconle.2008.12.002.

[25] A. Ilka and V. Veselý, "Gain-Scheduled MPC Design for Nonlinear Systems with Input Constraints," *IFAC-Pap.*, vol. 48, no. 11 11, pp. 912–917, 2015, doi: 10.1016/j.ifacol.2015.09.307.

[26] A. E. El-Sharkawy, J. C. Kamrad, T. H. Lounsberry, G. L. Baker, and S. S. Rahman, "Evaluation of Impact of Active Grille Shutter on Vehicle Thermal Management," *SAE Int. J. Mater. Manuf.*, vol. 4, no. 1, pp. 1244–1254, 2011, doi: 10.4271/2011-01-1172.

[27] V. Shigarkanthi, V. Damodaran, D. Soundararaju, and K. Kanniah, "Application of design of experiments and physics based approach in the development of aero shutter control algorithm," *SAE 2011 World Congr. Exhib.*, 2011, doi: 10.4271/2011-01-0155.

[28] W. H. Kwon and S. Han, *Receding Horizon Control*. London: Springer-Verlag, 2005. doi: 10.1007/b136204.
[29] A. Zhakatayev, B. Rakhim, O. Adiyatov, A. Baimyshev, and H. A. Varol, "Successive linearization based model predictive control of variable stiffness actuated robots," in *2017 IEEE International Conference on Advanced Intelligent Mechatronics (AIM)*, Jul. 2017, pp. 1774–1779. doi: 10.1109/AIM.2017.8014275.
[30] A. Dhar and S. Bhasin, "Adaptive MPC for Uncertain Discrete-Time LTI MIMO Systems with Incremental Input Constraints," *IFAC-Pap.*, vol. 51, no. 1, pp. 329–334, Jan. 2018, doi: 10.1016/j.ifacol.2018.05.040.
[31] D. F. Griffiths and D. J. Higham, "Numerical Methods for Ordinary Differential Equations," in *Numerical Methods for Ordinary Differential Equations*, Springer, London, 2010, pp. 19–31.
[32] D. E. Huntington and C. S. Lyrintzis, "Improvements to and limitations of Latin hypercube sampling," *Probabilistic Eng. Mech.*, vol. 13, no. 4, pp. 245–253, Oct. 1998, doi: 10.1016/S0266-8920(97)00013-1.

APPENDIX A

Table 8: System property values and units

System Model Property	Numeric Value	Units
$c_{p,air}$	1.005	kJ/kgK
ρ_a	1.204	kg/m^3
V	0.00018	m^3
m_H	1.505	kg
c_H	0.910	kJ/kgK
A_s	3.022	m^2
F_{fin}	0.898	$unitless$
η_{FA}	0.974	$unitless$
A_{fan}	0.1	m^2
r_m	0.0971	m
A_{fr}	2.592	m^2
$c_{p,air}$	1.005	kJ/kgK

The curve fits created for the refrigerant thermodynamic properties are in section 2.2.6:

$$T_{ref,c} = 2.06 \cdot 10^{-8} p_c^3 - 6.04 \cdot 10^{-5} p_c^2 + 0.109 p_c - 27.7 \quad (44)$$

$$T_{ref,e} = 2.25 \cdot 10^{-7} p_e^3 - 3.07 \cdot 10^{-4} p_e^2 + 0.235 p_e - 39.9 \quad (45)$$

$$h_{out,c} = h_{in,e} = 2.39 \cdot 10^{-8} p_c^3 - 7.04 \cdot 10^{-5} p_c^2 + 0.139 p_c + 163 \quad (46)$$

$$h_{out,e} = 1.59 \cdot 10^{-7} p_e^3 - 2.20 \cdot 10^{-4} p_e^2 + 0.166 p_e + 338 \quad (47)$$